applied sciences

MDPI

Article

Towards A Geo-Hydro-Mechanical Characterization of Landslide Classes: Preliminary Results

Federica Cotecchia [1], Francesca Santaloia [2] and Vito Tagarelli [1,*]

1 DICATECH, Polytechnic University of Bari, 4, 70126 Bari, Italy; federica.cotecchia@poliba.it
2 IRPI, National Research Council, 4, 70126 Bari, Italy; f.santaloia@ba.irpi.cnr.it
* Correspondence: vito.tagarelli@poliba.it; Tel.: +39-3928654797

Received: 21 September 2020; Accepted: 4 November 2020; Published: 10 November 2020

Abstract: Nowadays, landslides still cause both deaths and heavy economic losses around the world, despite the development of risk mitigation measures, which are often not effective; this is mainly due to the lack of proper analyses of landslide mechanisms. As such, in order to achieve a decisive advancement for sustainable landslide risk management, our knowledge of the processes that generate landslide phenomena has to be broadened. This is possible only through a multidisciplinary analysis that covers the complexity of landslide mechanisms that is a fundamental part of the design of the mitigation measure. As such, this contribution applies the "stage-wise" methodology, which allows for geo-hydro-mechanical (GHM) interpretations of landslide processes, highlighting the importance of the synergy between geological-geomorphological analysis and hydro-mechanical modeling of the slope processes for successful interpretations of slope instability, the identification of the causes and the prediction of the evolution of the process over time. Two case studies are reported, showing how to apply GHM analyses of landslide mechanisms. After presenting the background methodology, this contribution proposes a research project aimed at the GHM characterization of landslides, soliciting the support of engineers in the selection of the most sustainable and effective mitigation strategies for different classes of landslides. This proposal is made on the assumption that only GHM classification of landslides can provide engineers with guidelines about instability processes which would be useful for the implementation of sustainable and effective landslide risk mitigation strategies.

Keywords: landslide mechanism; phenomenological interpretation; numerical modelling; landslide risk; landslide classification; sustainable mitigation measures

1. Introduction

Landslides are still one of the main sources of risk for civil society [1–3], despite the widening of knowledge about their processes and the multiple initiatives aimed at risk mitigation. Landslides still cause numerous deaths and huge economic losses, impacting the socio-economic development of several regions, as is the case for large areas of the Italian peninsula (Figure 1; [4]). Given the current scenarios of the effects of landslides across the world, the most important international agendas (e.g., the Sendai Framework; Global Assessment Report 2019—GAR19) categorize landslides as natural processes which may cause 'disasters' for the civil society, and request the adoption of scientific methods in the assessment of the landslide risk and in the selection of mitigation measures, in order to guarantee the sustainability of the landslide risk management.

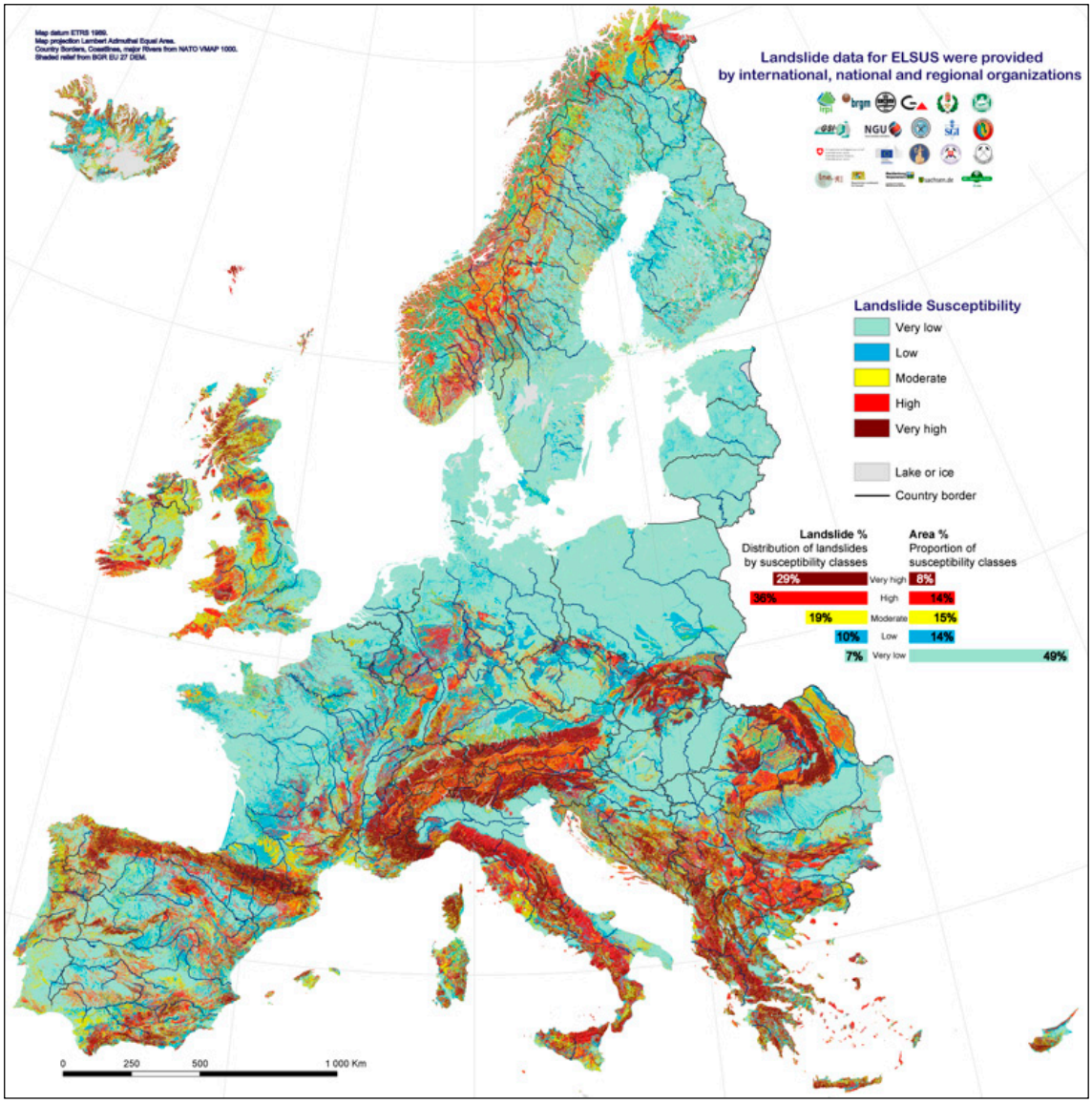

Figure 1. Landslide susceptibility map of Europe [4].

The background of the present paper is long-term research addressing the definition of design strategies for sustainable landslide risk mitigation [5–11]. The results of the background research have shown that sustainable landslide risk mitigation measures need to be based on an objective characterization of the landslide mechanism, i.e., of the slope failure processes and of their causes (either predisposing or triggering; [10–13]). Accordingly, the results of the background research provide evidence of why: (i) the characterization of landslide mechanisms is useful for geo-hydro-mechanical (GHM) studies of the slope features and equilibrium conditions; (ii) the routine selection of sustainable landslide risk mitigation measures would greatly benefit from the availability of a general framework of landslide mechanisms. This framework should result from a systematic characterization of landslide case histories through GHM studies and might develop into a GHM classification of landslides. This would represent an important step forward with respect to the geomorphological classification of landslides (e.g., [14–16]; Figure 2), which is, to date, the most complete and widely used approach. Such classifications have resulted from comprehensive field studies of landslide processes, carried out from the 1970s to 1990s, and have been of great significance to engineering practices, providing engineers with hints about the possible typology of the landslide process taking place on a given slope. However, the authors of this classifications clearly stated that the landslide classes were characterized mainly

through geomorphological studies and, as such, they did not provide comprehensive information concerning the hydro-mechanical causes and processes determining the progression of slope failure. Therefore, such classifications cannot provide objective assessments of landslide causes which may be accounted for in the design of mitigation strategies. Hence, the integration of such geomorphological landslide classifications with GHM characterizations of landslide mechanisms would prove to be a powerful support to the professional community involved in the selection and design of landslide risk mitigation measures.

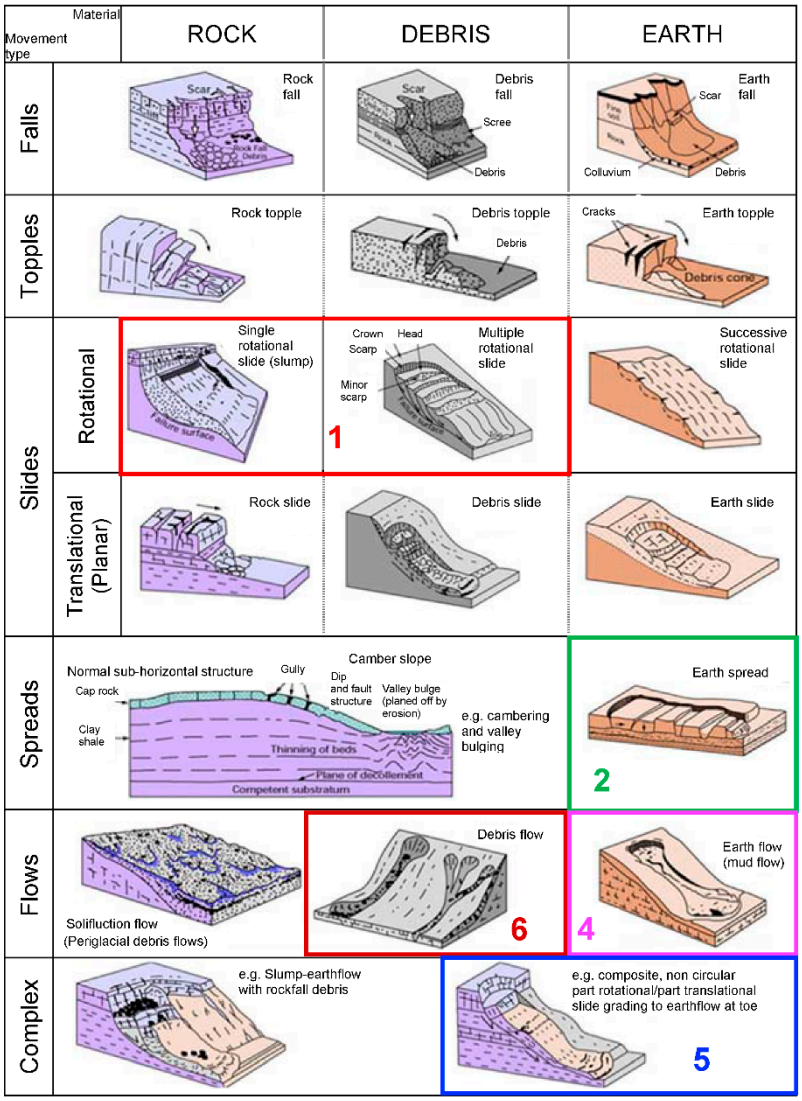

Figure 2. Landslide classification ([16]; https://www.bgs.ac.uk-British Geological Survey).

With these notions in mind, this paper presents the preliminary results of research seeking to address, in the long term, the above-mentioned integration of the available geomorphological classification of landslides, and should ultimately result in a system which could be defined according to GHM classifications of landslides. Accordingly, the paper reports a first tentative GHM characterization of some of the landslide classes of the Cruden DM and Varnes DJ geomorphological classification [16] (Figure 2): (1) rotational-rototranslational slides (box 1 in Figure 2); (2) lateral spread-flowslides (box 2 in Figure 2); (3) compound landslides [15], not shown as a class in Figure 2, but which could be a subset of the complex landslides depicted in the Figure; (4) earthflows (box 4 in Figure 2); (5) deep mixtilinear slides (box 5 in Figure 2); and (6) debris flows and debris flowslides (box 6 in Figure 2). Such a characterization was based on the results of several studies reported in the literature which

provided GHM interpretations of landslide case histories, through phenomenological, conceptual, or numerical models of the mechanism.

First, this paper briefly describes the methodology which is generally adopted for GHM characterizations of landslide mechanisms, defined as "stage-wise" by Cotecchia et al. [10]. Thereafter, the paper presents the literature database used for tentative GHM characterizations of the six landslide classes cited above. Finally, the synthetic GHM characterization of such classes is discussed.

2. The Stage-Wise Methodology for the GHM Characterization of the Landslide Mechanisms

Assessments of landslide mechanisms, traditionally carried out at the slope scale, integrate data characterizing the variables controlling the slope stability, as defined by Terzaghi [17], as internal and external landslide factors (Figure 3), within the framework of the physical laws that control the slope movements [10] in connection with external factors, i.e., the landslide mechanism (Figure 4). Figure 5 illustrates the main steps of the GHM analysis of the slope processes determining the landslide mechanism, which are primarily hydro-mechanical. Such an analysis can now benefit from the considerable development which has occurred in recent years of the techniques of surveying and monitoring of landslide factors (in the fields of topography and geomatics, sensor technology and digital communication), and of the digital-based construction of databases [18,19]. Moreover, GHM analyses can now implement advanced physical-mathematical modelling of slope responses to external factors, providing knowledge about the internal and external causes of the landslides, whose identification is a prerequisite of the proper design of sustainable landslide mitigation measures [10,20].

For slopes consisting mainly of soil, which are a reference in the present paper, the 'first failure' mechanism [12,16,21] can be modelled within the theoretical framework of continuum mechanics by means of several numerical strategies [22–26]. These are aimed at simulating the coupling between the physical (hydro-mechanical and thermodynamic) and chemical phenomena that control the slope response, in terms of a boundary value problem ([10]; Figure 5c). This is quoted to provide a perspective of how comprehensive a GHM analysis may become; moreover, in some peculiar cases, a proper and successful landslide diagnosis may necessitate taking thermal or chemical behavior into account. Hence, generally speaking, this modelling requires the solution of a system of differential equations which is representative of the phenomena controlling the slope equilibrium over time, whose number varies depending on the number of processes accounted for in the modeling. In order to predict the displacement field over time, it is necessary to integrate a system including at least the equilibrium equation (which implements the elasto-plastic constitutive law of the slope soils) and the conservation equation of pore fluid masses ([22,27,28]; Figure 5c), i.e., either liquid or gas. Through the solution of such a system, the modelling predicts the strain field propagation up to the 'onset' of a landslide, and provides knowledge about both the morphology and the kinematics of the landslide (style and distribution of landslide activity; [16]), as well as about its causes.

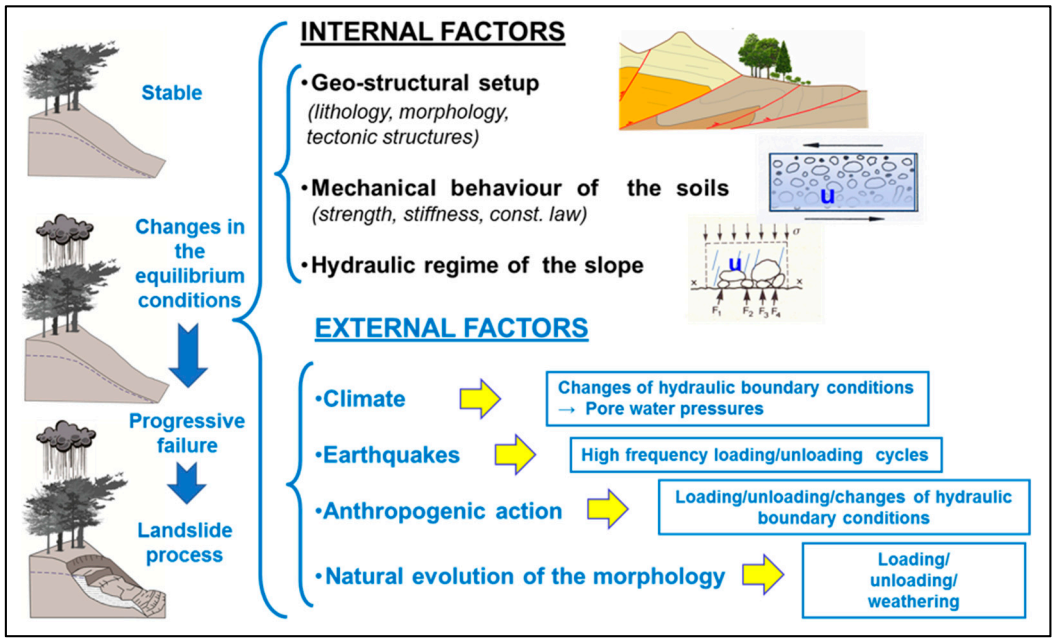

Figure 3. Landslide factors [17].

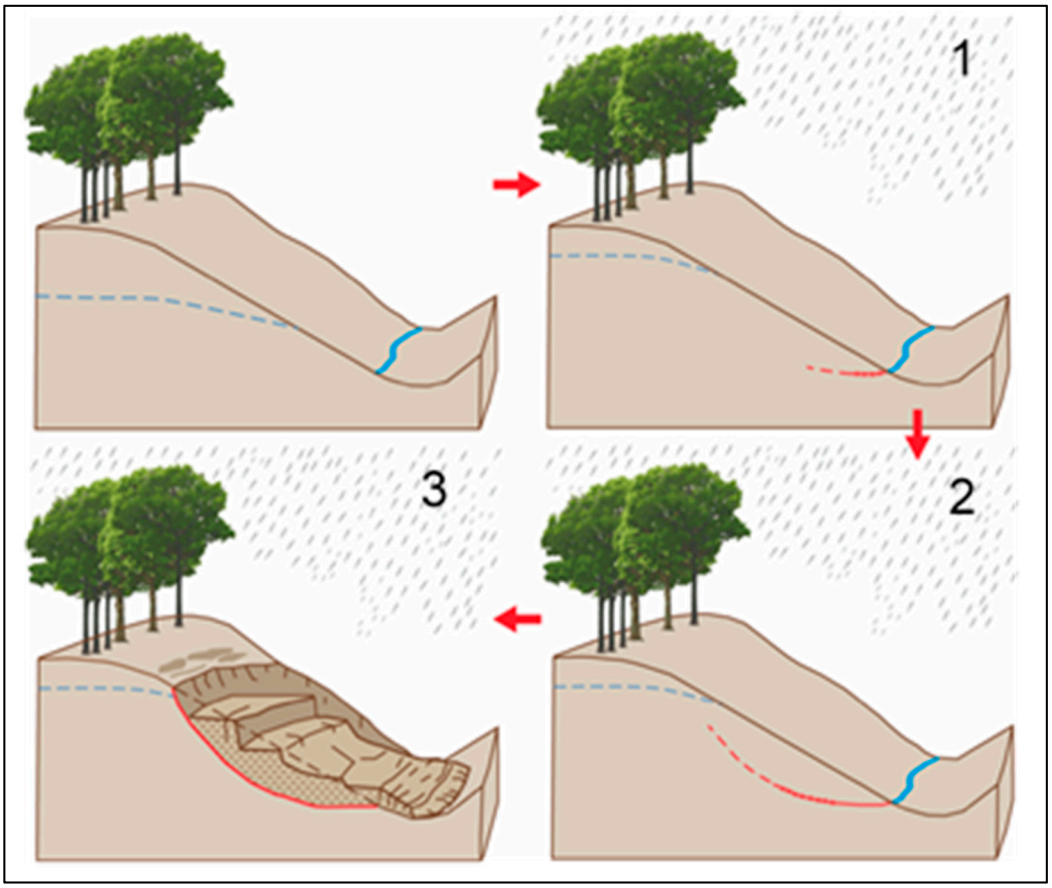

Figure 4. Landslide mechanism: from the triggering action (**1**), through the development of the shear band (**2**) until the final mobilization of the landslide body (**3**).

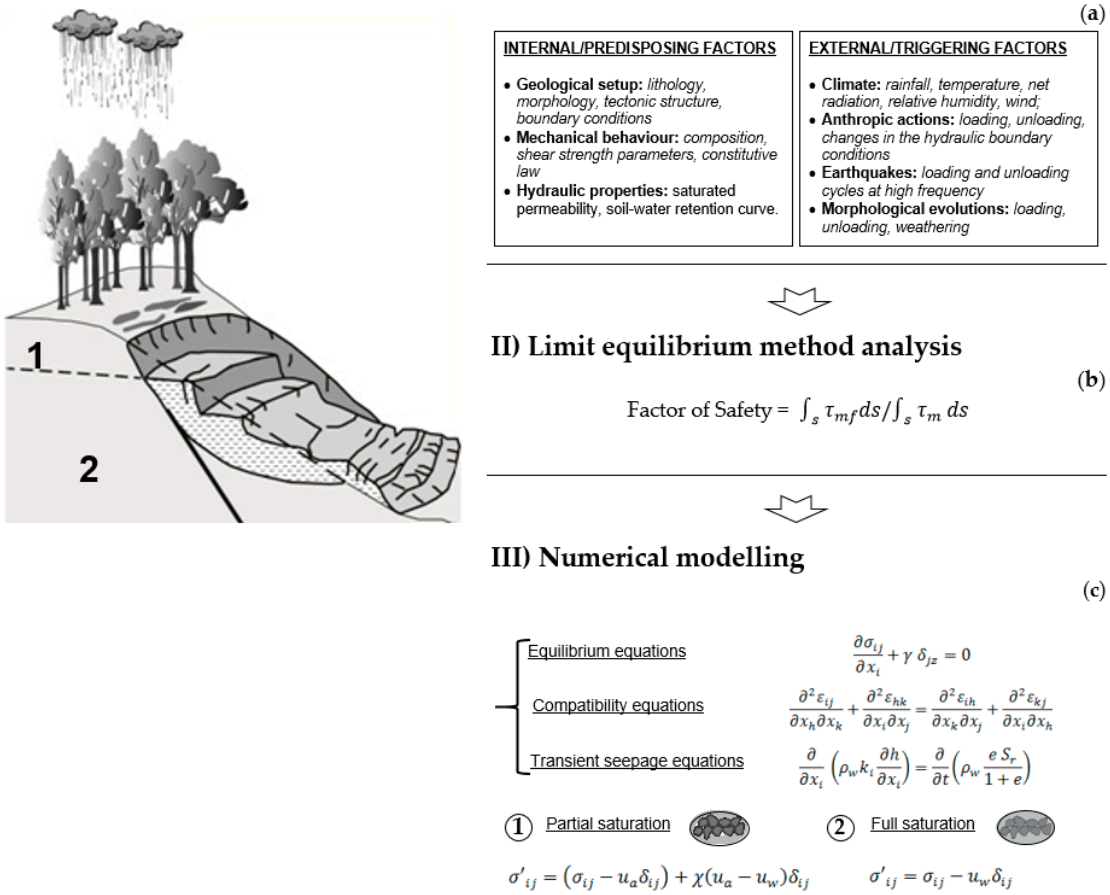

Figure 5. The stage-wise methodology for the GHM characterization of the landslide mechanisms [10]. (**a**) Phenomenological diagnosis, I level of analysis; (**b**) limit equilibrium method, II level of analysis; (**c**) numerical modelling, III level of analysis.

In synthesis, when an external action occurs, the stress state across the slope changes over time, satisfying the equilibrium and strain compatibility, while determining strain localizations whose distribution depends on the hydro-mechanical properties of the slope materials and on the boundary conditions. As the straining develops over time, the mobilization of the landslide body progresses, with the development of a major discontinuity within the displacement field. In general, the so-called landslide event matches a stage when the difference in displacement rate between a slope portion (i.e., the landslide body) and the rest of the slope becomes significant. The major discontinuities in the displacement field correspond to the strain localization regions, typically either traction bands, or shear bands. The shear band may become the location of a slip surface. Therefore, the landslide event is the final paroxysmal episode of a deformation process across the slope, being defined as a progressive failure (Figure 5; [5,29–41]) which takes place before the first activation of the landslide body. When dealing with reactivation mechanisms, before the remobilization of the landslide body, the processes are similar to those of 'first failure' landslides, but the displacement field is strongly controlled by pre-existing shear bands (eventually of the material discontinuities).

The modelling of the landslide 'propagation' [42–45], instead, requires different analytical tools which depend on the type of landslide. In particular, for the six landslide classes discussed in this paper (Figure 2), different modelling strategies must be used to predict the propagation, whether they are: (i) slow landslides, whose displacement is limited [16]; or (ii) large propagation landslides, often fast [16,42], with propagation distances from hundreds of meters to kilometers (earthflows, mudflows, debris-flows and flows; [15,16]). The prediction of the landslide mass propagation can

still make use of continuum mechanics if the propagation ranges from decimeters to tens of meters in years (category (i)), according to analytical strategies which are similar to those used to predict ground settlements determined by tunnel excavations [46], eventually adopting computational methods accounting for large straining. For the landslides in category (ii), instead, the propagation modeling should involve the use of either discrete element codes [24,47–50] or numerical codes that consider the soil mass as a viscous fluid [51–55] of high granular content [56–58].

Despite improvements in slope numerical modelling, it should be pointed out that the coupled modelling of all the processes active in slopes is still a scientific challenge. Therefore, numerical modelling should account for the slope factors and physical laws which are active in the slope (Table 1) according to their level of influence on the landslide mechanism. To this end, numerical modelling should be always preceded by experimental analyses of the slope processes performed in the field [14,15], supported by advanced monitoring devices. It follows that neither phenomenological analyses nor numerical modelling alone can provide reliable assessments of landslide mechanisms; rather, a stage-wise methodology which starts with phenomenological studies in the fields of geology, geomorphology, and geotechnics (in the field and the laboratory) should be routinely implemented to deduce the most important aspects of reliable quantitative modelling of landslide mechanisms. In particular, as illustrated in Figure 5, the methodology should be composed of three stages: the first (I), aimed at the identification of the slope factors (Table 2) and the phenomenological interpretation of the landslide mechanism; the second (II), when a simplified quantitative analysis of the slope stability is carried out through the limit equilibrium method, for a first check of the phenomenological interpretation obtained in the first stage; and the third (III), representing the numerical analysis, in which the boundary value problem is solved by means of numerical modelling, in the context of a geotechnical model constructed on the basis of the results of the previous stages. An exhaustive discussion of the stage-wise methodology is reported in [10,11,59].

Table 1. Laws and equations controlling the thermo-hydro-mechanical state of the soils in the slope (after [20] modified).

	Balance Equations	**Variables (Unknowns)**	**Physical Laws and Constitutive Properties**	**Boundary Conditions**
COUPLED HYDRO-MECHANICAL - HM COUPLED THERMO-HYDRO-MECHANICAL - THM COUPLED THERMO-HYDRAULIC - TH UNCOUPLED HYDRAULIC - H	Mass balance of liquid: liquid water and air dissolved in water (H balance)	P_l	• Darcy's law • Fick's law • Henry's law • Psychrometric law • Ideal gas law • Retention curve • Conductivity functions • Diffusion/Dispersion coefficients	Pressures/Fluxes /Meteorological factors
	Mass balance of gas: water vapour and air (G balance)	P_g		
	Internal energy balance (T balance)	T	• Fourier's law • Thermal conductivity • Density variation with T	Temperatures/ Fluxes
	Momentum balance (M balance)	u	• Soil constitutive model and corresponding parameters	Displacements/ Forces

Table 2. Macrocategories of data to be acquired in the context of analyses and surveys.

(1).	Historical data and indications of displacements and instability of the slope in the past, damage, etc. (*)
(2).	Topographic data
(3).	Vegetation cover and land use data
(4).	Data from geomorphological surveys: changes of local sloping angle due to excavation, erosion, (*) morphologies caused by instability related to the current landslide process or past processes (e.g., main and internal scarps, accumulation areas, channel areas, detachment niches, etc.).
(5).	Data from geo-structural survey of discontinuities
(6).	Surficial lithostratigraphic, geological and geo-structural data (map of outcrops and covers, map of tectonic features)
(7).	Deep lithostratigraphic and geo-structural data, description of the geotechnical corings
(8).	Index properties and hydro-mechanical parameters of the lithotypes, from geotechnical testing, either in situ, or in the laboratory
(9).	Hydro-geological boundary conditions of the slope: feeding and drainage areas
(10).	Piezometric data
(11).	Superficial and deep displacements (e.g., inclinometric data), with the possible identification of pre-existing shear bands linked with the morphology of active landslide bodies (*)

(*) Referring to data that can be acquired only if the landslide mechanism is either active or it has already been active in the past.

Two Examples of the Application of the Stage-Wise Methodology

Hereafter, the application of the stage-wise methodology to diagnose landslide mechanisms is presented for two case studies, the Pisciolo and the Tolve landslides. In both cases, the landslides are part of a landslide basin, including multiple rototranslational, slow-moving landslide bodies, of medium to high depth [15]. These examples are presented to exemplify how to apply the stage-wise methodology, which is the key pivot to gather GHM characterization data aimed at a comprehensive diagnosis of any landslide mechanism.

At Pisciolo, the landslide involved fissured clays incorporating floating fractured rock blocks, whereas at Tolve, it involved stiff, highly overconsolidated and locally weathered clays, as shown in Figures 6 and 7, respectively. At both sites, the study was started according to the prescriptions for stage I of the methodology in Figure 5, i.e., carrying out geological and geomorphological field surveys of the whole landslide basin, multitemporal photointerpretation of the hillslope, investigation of the slope at depth through continuous coring and undisturbed geotechnical sampling down to large depth, geophysical surveys (in particular geoelectric tomography), analysis of the soil corings and of the results of geotechnical laboratory tests on the undisturbed soil samples, and topographic monitoring. These activities allowed us to phenomenologically interpret the slope instability processes at the sites. Thereafter, in stage II, a back-analysis of the limit equilibrium of the different active sliding bodies (safety factor F = 1) was carried out, implementing the geological, geotechnical and piezometric data stage I, in order to check the stage I phenomenological interpretation of the landslide, in particular, deriving a hierarchy of instability among the different landslide bodies. Finally, the diagnoses of the landslide mechanisms were verified by means of coupled hydro-mechanical modelling (using the finite element method, FEM) of the slope, according to stage III of the methodology. Such numerical analyses allowed us to verify the landslide diagnoses achieved through stages I and II, and to define a slope model for use in the design of mitigation measures.

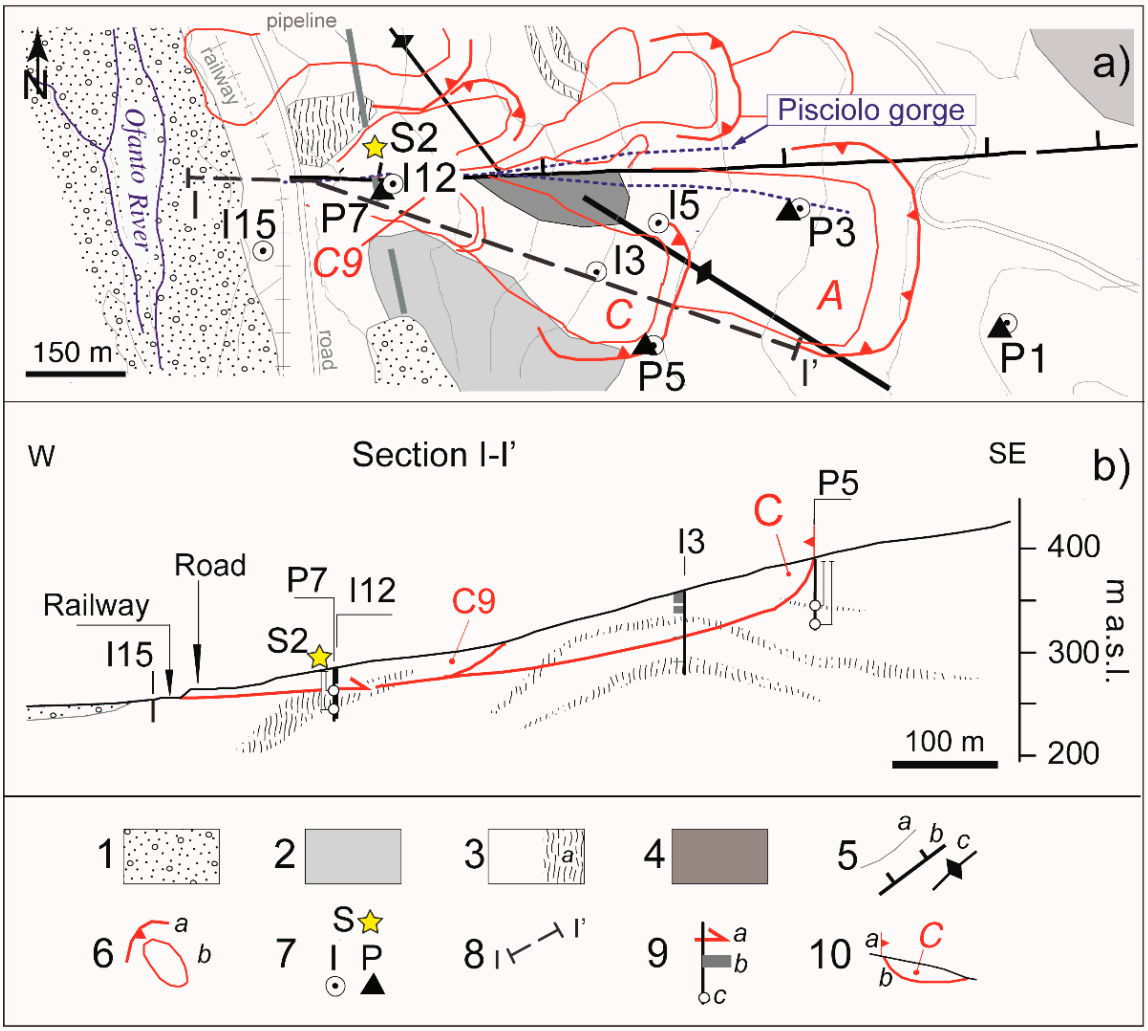

Figure 6. Geological map (**a**) and section (**b**) of the Pisciolo slope (modified from [40]). Key: (1) debris and alluvial deposits; (2) Numidian Flysch; (3) Paola Doce clays, and fractured rock inclusions (a); (4) Red Flysch; (5) stratigraphic contact (a), fault (b) and anticline axis (c); (6) landslide crown (a) and body (b); (7) borehole with piezometers (P), borehole with inclinometer (I), GPS sensor (S); (8) line of section; (9) inclinometer shear bending (a), disturbed soil (b) and piezometer cell with corresponding hydraulic heads (c); (10) labelled landslide: crown (a), slip surface (b).

For the Pisciolo slope, based upon the Stage I analyses, the low values of the strength parameters characterizing the clays at any depth in the slope, together with the high piezometric levels (in the range of 2 m–5 m below the ground level in most part of the hillslope, even at large depth) were recognized as predisposing factors for a landslide. In particular, the high piezometric levels were shown to be connected to the slope-scale permeability, which was higher than typical values for clay slopes, since the Pisciolo slope clays are highly fissured and include coarser soil strata and fractured rock blocks (Figure 6), which, on the whole, increase rainfall infiltration rates. Accordingly, the piezometric monitoring data show that the slope hydraulic features, combined with the climatic regime of the area, bring about a transient seepage in the slope that, down to large depths, determines seasonal variations of the piezometric heads, which influence slope stability. In particular, monitoring displacements at depths from a few meters to 40–50 m and the use of piezometric heads gives evidence of the occurrence of both a mild rate of increase of the piezometric heads and a mild acceleration of the landslide bodies from late autumn to late winter/early spring, with both the maximum piezometric heads and maximum the displacement peak rates occurring in early spring ([10,40,41]; Figure 8). It follows that the stage

I data suggest that the landslide activity at Pisciolo is climate-induced and, hence, is connected to slope-vegetation-atmosphere interactions.

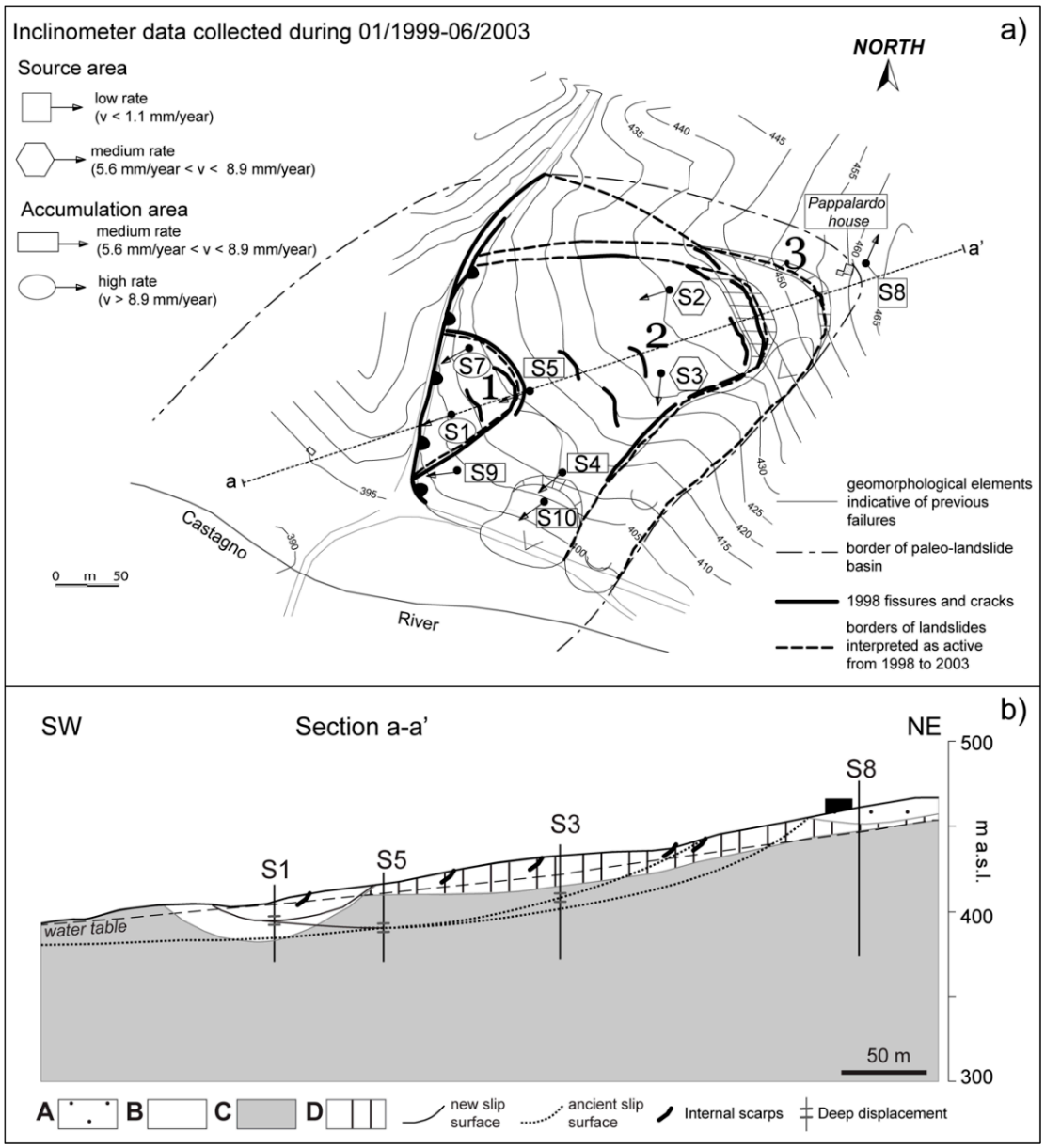

Figure 7. Geomorphological map (**a**) and section (**b**) of the Tolve slope (adapted from [60]); Key. Soil complexes: yellow sands (**A**), remoulded clays (**B**), sub-Apennine Clays (**C**), weathered clays (**D**).

Elia et al. [20] reviewed the mathematical laws which are useful to represent the hydraulic, mechanical and thermodynamic processes which evolve in slopes as an effect of both the climate and vegetation, and which, on the whole, are able to describe slope-vegetation-atmosphere interactions. The authors reported the various modeling strategies of such interactions, which account for different coupling degrees. For the Pisciolo case study, the slope-atmosphere-vegetation interaction was simulated, first through hydraulic (H) uncoupled FEM modelling (Figure 9, [40,61]), inputting net rainfall rates at the top boundary of the slope model, calculated as the difference of the total rainfall rate and the evapo-transpiration rate estimated by means of the FAO-Penman-Monteith method [62]. This hydraulic modelling, combined with the limit equilibrium analyses (Stage II), confirmed that seasonal slope-vegetation-atmosphere interaction lead to F = 1 by the end of winter/early spring in bodies deeper than 3 m [61,63–65]. At the same time, the analyses showed that the stability of landslide

bodies shallower than 1–2 m is connected to the intensity and duration of single rainfall events, or to their short-term sequences from mid-autumn to mid-spring ([61]; Figure 9). The research results, therefore, highlight the variability with depth of climatic variables, which the landslide body stability relates to in clay slopes similar to the Pisciolo slope.

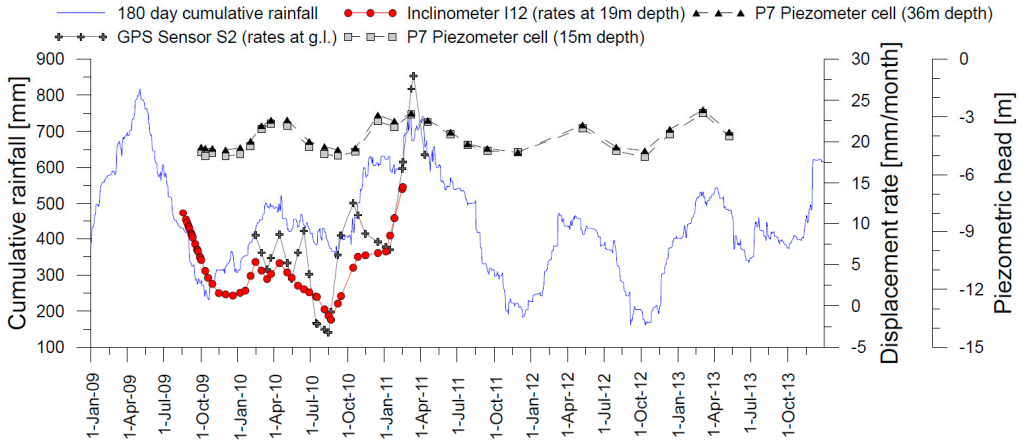

Figure 8. Pisciolo slope—180-day cumulative rainfalls and monitoring data (after [40]); for the piezometric head z = 0 at ground surface; the location of the piezometers and inclinometers cited in the legend are shown in Figure 6.

Pedone [66], Tagarelli [64] and Tagarelli and Cotecchia [67] also reported the results of stage III analyses of the Pisciolo slope, carried out using fully coupled hydro-mechanical (HM) FEM modelling of the slope-vegetation-atmosphere interactions. Tagarelli and Cotecchia [67] reported two-dimensional coupled HM numerical analyses of the slope-vegetation-atmosphere interaction, but assumed the slope to be homogeneous and checked the influence of the model initialization procedure on the prediction of the slope-vegetation-atmosphere interaction. The authors concluded that only when the slope model initialization accounted for the slope loading history, including that determined by the excavation of the river valley and the consequent formation of the slope, could the numerical analyses predict that even a homogeneous slope formed by an elasto-plastic, nonhardening clay may become location of a climate driven landslide.

For the Tolve slope, Cotecchia et al. [41,60] diagnosed the landslide mechanism determined through a small size excavation at the slope toe using a stage-wise methodology. Temporal geomorphological analyses [68] allowed them to recognize that the slope is part of a large paleo-landslide basin, having its original toe at the Castagno River, at the foot of the valley (Figure 7). Given the study of the slope stratigraphy, showing that the slope is mainly formed from sub-Apennine stiff clays, and the monitoring of the deep displacements (through inclinometers) and of the piezometric head, the authors recognized that the current landslide largely represents a reactivation of sliding, rather than the effect of a first failure process. In this slope, the first failure of the clays took place after excavation only in a limited region, where a new shear band developed, linking the bottom of the excavation with the pre-existing shear band at depth. Given this phenomenological interpretation of the landslide mechanism achieved through stage I studies, both the stage II and III analyses confirmed how a small excavation along the longitudinal axis of a paleo-landslide body can to trigger the delayed reactivation of large portions of part of this body, due to the new yielding of the slope clay triggered by the excavation, which starts at the floor and develops progressively over time until the original shear band lying at depth is reached. As a consequence, the new landslide activity is characterized by mass movements whose size and direction differ from those of pre-existing landslides. A stage III FEM analysis of the slope processes predicted the reactivation of sliding at Tolve after the completion of consolidation pos-excavation once a pre-existing shear band, which includes clay weaker than the undisturbed stiff clay, is implemented in the model [41,60]. Figure 10 shows the onset of yielding at the toe of the excavation soon after the excavation and its development with negative consolidation.

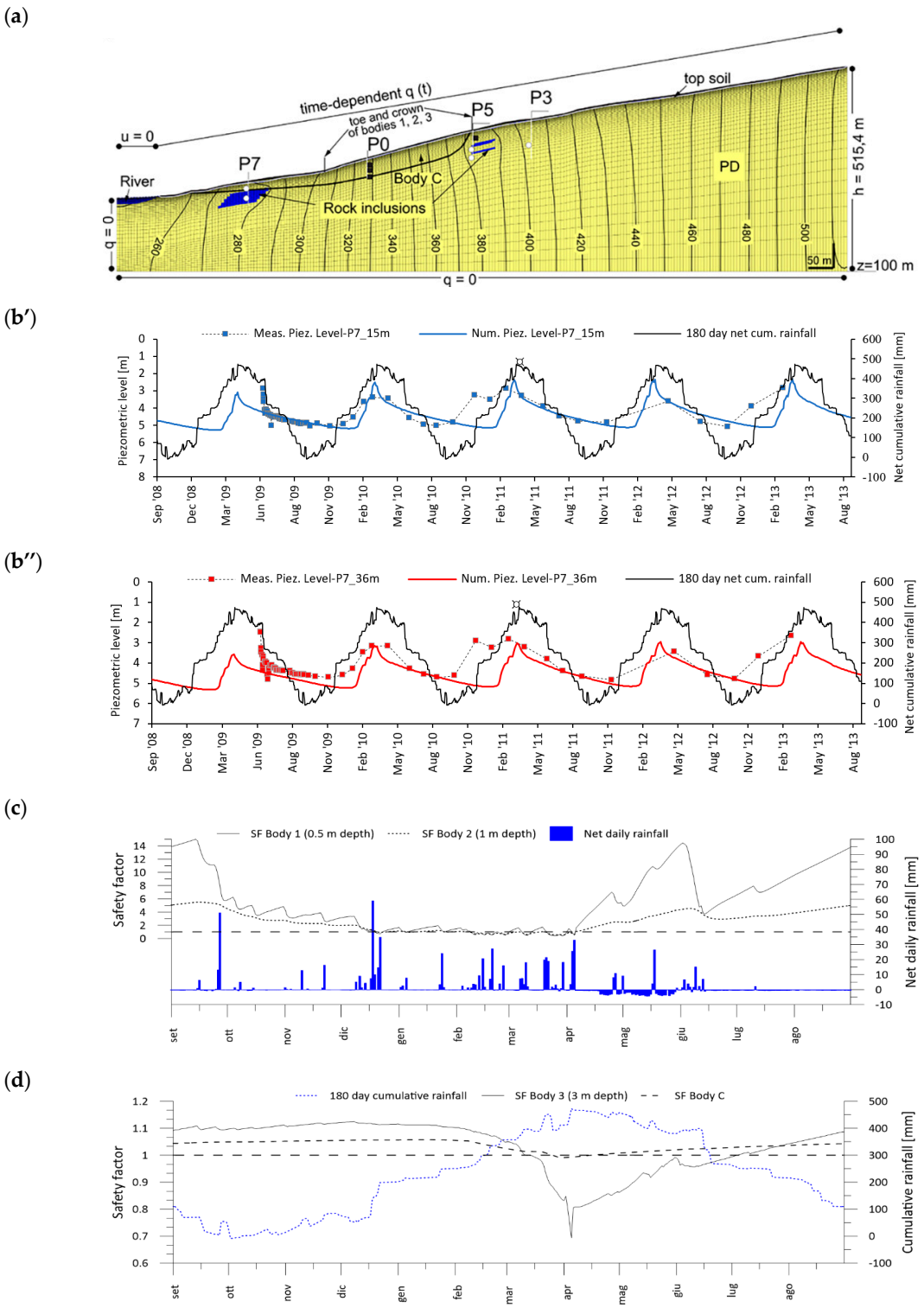

Figure 9. Hydraulic modelling and limit equilibrium analysis of the slope-vegetation-atmosphere interaction for the Pisciolo slope: (**a**) FE slope model, boundary conditions and equipotential lines at the end of the steady state hydraulic modelling; results of the hydraulic modelling: hydraulic heads for the piezometric cell, along the vertical P7 (Figure 6), at 15 m (**b′**) and 36 m (**b″**) compared with monitoring data (blue and red dots) together with 180-day net cumulative rainfall; results of the limit equilibrium analysis: (**c**) safety factor (SF) variation during the year for shallow landslide bodies, together with the daily net rainfall; (**d**) safety factor (SF) variation during the year for deep landslide bodies together with the 180-day cumulative rainfall; (modified after [40,61]).

Despite the simplifications inherent to the slope models for both the Pisciolo and the Tolve case studies, in both cases, the stage III numerical modelling was able to reproduce the landslide mechanism observed in situ, validating the phenomenological diagnosis formulated through stage I studies. As for the Pisciolo and the Tolve landslides, the literature reports several examples of similar applications of the stage-wise methodology, along with consequent diagnoses (Figure 5; [5,9,10,38,41,44,69–75]).

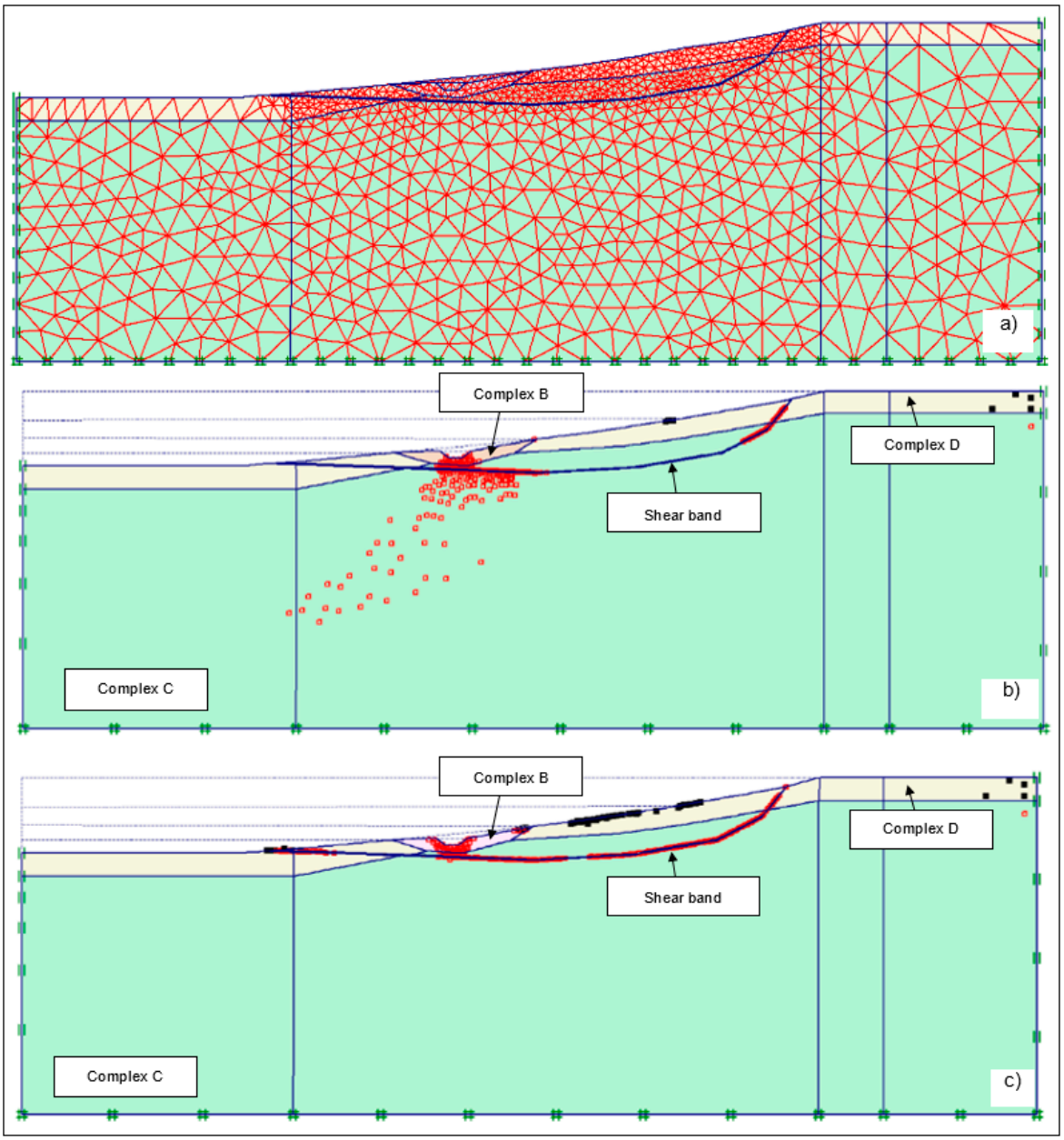

Figure 10. FEM analysis of the Tolve slope (modified from [76]): slope after excavation (**a**), yield points at the end of the undrained excavation (**b**) and at the end of the coupled consolidation, before the occurrence of numerical instabilities (**c**); stages (**b**,**c**) performed implementing weak soils in complex B ($c' = 6$ kPa; $\phi' = 24°$) and in the shear band ($c' = 0$ kPa; $\phi' = 16°$).

3. GHM Characterization of the Landslide Classes: A Preliminary Attempt

Hungr et al. [42,77], among others, developed the classification of landslides, from the perspective of geo-mechanical classification, by integrating some mechanical features of the landslide mechanisms with the geomorphological aspects of reference in previous classification systems (e.g., [14–16]; Figure 2). Moving towards a similar perspective, in this section, a methodology to derive a GHM characterization

of landslide classes is proposed. Furthermore, a tentative GHM characterization is presented of the six landslide classes presented in the introduction by referring to Cruden and Varnes classification [16] (Figure 2), as indicated, through corresponding schemes, in Figure 11. Such an attempt was the result of an initial application of the proposed methodology, and sheds some light on the most typical factors and processes controlling the landslide mechanisms being part of these classes.

The methodology starts with a detailed analysis of the hydro-mechanical features of the landslides in each of the six geomorphological landslide classes (Figure 2). Hence, the methodology stems from the awareness that the fundamental laws controlling the slope response to external factors, and the eventual slope failure, are basically those reported in Table 1 (if seismic actions are excluded). Therefore, it is plausible that each landslide class may be related to a limited number of combinations of landslide factor values and boundary conditions. Given this, the collection, for each landslide class, of the landslide factor values and boundary conditions recorded in GHM studies of landslides belonging to a given class should bring about the characterization of the predisposing and triggering causes which are most recurrent for that landslide class. Also, the reasons for the variability in size and morphology of the landslide bodies typical for the given class should be derivable. Consequently, for each landslide class, the methodology requires an accurate review of case studies referring to landslides belonging to that class, within which landslide factors have been exhaustively characterized and landslide mechanisms assessed through either stage I, or II and III analyses (Figure 5). Such a literature review is expected to serve in the identification of repetitive connections between sets of values of landslide factors and given landslide mechanisms.

With the aim of both providing a detailed presentation of the methodology and exemplifying its application, the preliminary results are presented; these results were achieved through the application the methodology for the six landslide classes cited above (Figure 11). In particular, the sets of landslide factor values are illustrated which, in broad terms, were found to recur for these landslide classes, based upon the study of the literature carried out so far.

Each of Tables 3–8 corresponds to one of the six selected landslide classes, and reports the values of the main landslide factors measured in the different case studies in the literature, along with information about the boundary conditions. In particular, the values characterizing the geological (geological formations, lithological sequences, tectonic structures, landslide activity, e.g., first-time failure or reactivated landslide), hydraulic (piezometric levels and saturated permeability coefficients) and mechanical (soil granulometry, index properties, shear strength parameters) slope factors are presented in the tables, together with the boundary conditions (either hydraulic or mechanical). It is worth noting that the GHM characterization proposed here for the six classes (Tables 3–8) represents the outcome of an initial application of the methodology, and will be largely improved through a more extensive literature review and the performance of new field diagnoses, using the stage-wise methodology (Figure 5). Hence, what is discussed in the following should be considered mostly as a methodological contribution.

To start with, the application of the methodology to class 1, which includes rotational and rototranslational landslides, often evolving into multiple landslides (Figure 11, box 1 in Figure 2), will be discussed. For such landslides, the sliding surface is most often from circular to composite, and develops through a relatively thin shear band. For multiple landslides, it confines a deeper body within which other rototranslational landslide bodies are included, all sharing the same toe. The case studies examined for the GHM characterization of class 1 landslides were: the London Clay landslides, due to the delayed failure of cut slopes ([31]; Figure 12 [5]; Figure 13a, the Warden Point landslide [78,79]), some landslides in sub-Apennine Clays slopes (Figure 13b, the Petacciato landslide [80]; the Ancona landslide [81,82]; Figure 13c, the Lucera landslide [38]; Figure 7, the Tolve slope [60]), and the Selborne landslide in a Gault Clay slope (Figure 13d [83]). The factor values and the boundary conditions recorded for these landslide case studies were shown to be very similar (Table 3). The slopes are all mainly formed of a sequence of uniform marine clays, locally weathered in the upper part and covered by a thin coarse soil deposit of either marine or continental origin.

The clay is always of high consistency, since it is highly overconsolidated, and only mildly disturbed by tectonics. The more fissured portion of the clay is within the upper weathered portion of the slope. The original lateral earth pressure coefficient at rest (one-dimensional conditions), K_0, of the clays is generally higher than 1 [5,38,84,85]. Consistent with this, the response of the clay to shearing is initially very stiff, dilative and strain hardening until peak strength, becoming strain softening after peak. The peak shear strength parameter values range from medium (Lucera sub-Apennine Clays; London Clay) to relatively high (Petacciato and Ancona sub-Apennine Clays; Gault Clay). The decay in shear strength with straining brings the clay to a critical state, and thereafter, to residual (Table 3). The saturated permeability coefficient of the clay, K_s, is very low, i.e., about 10^{-11} m/s in the laboratory and about 10^{-10} m/s at the slope scale (field value; Table 3). Due to the low permeability at the slope scale and the hydraulic boundary conditions of the slopes of reference (absence of a lateral aquifer feeding the seepage in the slope), the piezometric levels at large depths are much lower than at shallow depths. Therefore, overall, the peak strength parameter values, together with relatively low pore water pressures at depth, provide the slope locations of landslides of class 1 with a significant stability factor when the slope angle is low to medium. Accordingly, most of these landslides resulted from first-time failures triggered by slope toe excavation, conferring upon the slope a much higher inclination. Such excavation was either of anthropic origin (e.g., London Clay slopes and Lucera slope in Table 3), or natural origin, e.g., due to marine erosion (Ancona, Petacciato and Warden Point slopes in Table 3) for the examined case studies. For instance, the first-failure process of the Petacciato landslide was triggered by marine excavation at the toe of the coastal slope, during the geological history of the area (Table 3; about 10,000–6000 years ago).

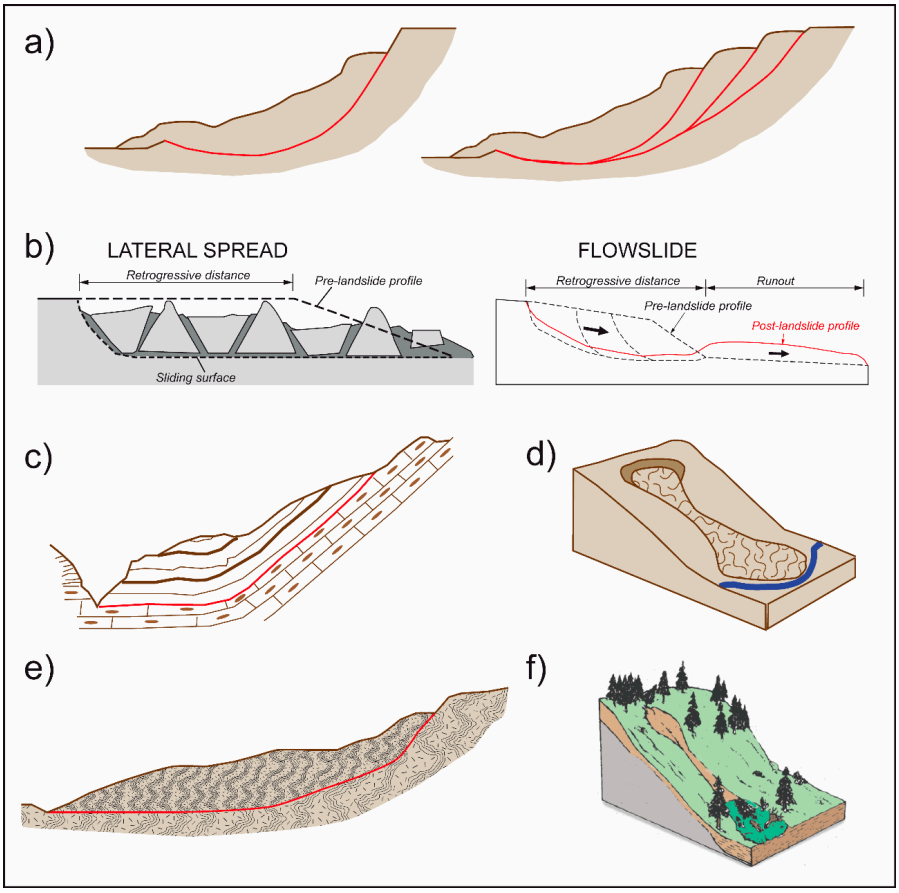

Figure 11. Classes of landslide mechanisms discussed in the paper. (**a**) Rotational-rototranslational slide; (**b**) Lateral spread and flowslide; (**c**) compound landslide; (**d**) earthflow; (**e**) deep mixtilinear slide; (**f**) debris flow and debris flowslide.

Table 3. Landslide factors of some landslide mechanisms belonging to class 1 (Figure 11); Key: CF—clay fraction, PI—Plastic Index, A—activity, peak shear strength (c'_p—cohesion, ϕ'_p—friction angle) e residual one (c'_r—cohesion, ϕ'_r—friction angle; [5,38,60,68,79,80,82,83,86–88]).

Landslide Factors		Lucera [38]	Ancona * [81,82]	Petacciato * [80]	Tolve * [60]	London Clay Slope Excavation [5,31]	Selborne Cutting [83]	Warden Point [78,79]
Geological	Formation	SC	SC	SC	SC	LC	GL	LC
	Tectonic structures	Fault and fold						
	First-time failure	Current	Quaternary	Quaternary	Quaternary	Current	Current	Current
	Reactivated failure	Current	Current	Current	Current			Current
Geotechnical	Classification	C_{sho}	C_{sho}	C_{sho}	C_{sho}	C_{sho}	C_{sho}	C_{sho}
	Grain-size data	CF = 41%	CF = 44%	CF = 41%	CF = 58%	CF = 55%	CF = 42%	CF = 43%
	Index properties	PI = 24.3%, A = 0.60	PI = 20%, A = 0.60	PI = 23%, A = 0.81	PI = 39%, A = 0.66	PI = 52%, A = 0.95	PI = 42%, A = 1.08	
	Shear strength parameters	c'_p = 30 kPa ϕ'_p = 22° ϕ'_r = 10°–12°	c'_p = 35–250 kPa ϕ'_p = 20°–28° ϕ'_r = 10°	c'_p = 0–160 kPa ϕ'_p = 18°–25° ϕ'_r = 10°	c'_p = 77 kPa ϕ'_p = 16° ϕ'_r = 10°	c'_p = 20 kPa ϕ'_p = 20° c'_r = 2 kPa ϕ'_r = 13°	<u>Weathered unit</u> c'_p = 10–15 kPa ϕ'_p = 24°–25° ϕ'_r = 13–14° <u>Unweathered unit</u> c'_p = 25 kPa ϕ'_p = 26° ϕ'_r = 15°	
	Permeability coefficient (m/s)	Field: 10^{-10} Lab.: 10^{-11}		Field: 10^{-7}–10^{-9} Lab.: 10^{-11}	Field: 10^{-8}–10^{-9} Lab.: 10^{-11}	Field: 10^{-9}–10^{-11} Lab.: 10^{-11}–10^{-13}		
Piezometric	Piezometric levels at large depth	Up and half slope: −10/−20 m p.c. Foot slope: −2 m p.c.	Up-slope: tens of metres below g.l. Down-slope: from g.l. to beyond g.l. (e.g., +7.1 m)	Up-slope: tens of metres below g.l. Middle and downslope: from g.l. to beyond g.l. (e.g., +4 m)	Few meters below g.l.	Steady-state seepage with water table at 2–3 m below g.l.		

(SC) sub-Apennine Clays, (LC) London Clay, (GC) Gault Clay, (C_{sho}) stiff and highly over-consolidated clay, * paleo-landslide sub-class, (g.l.) ground level.

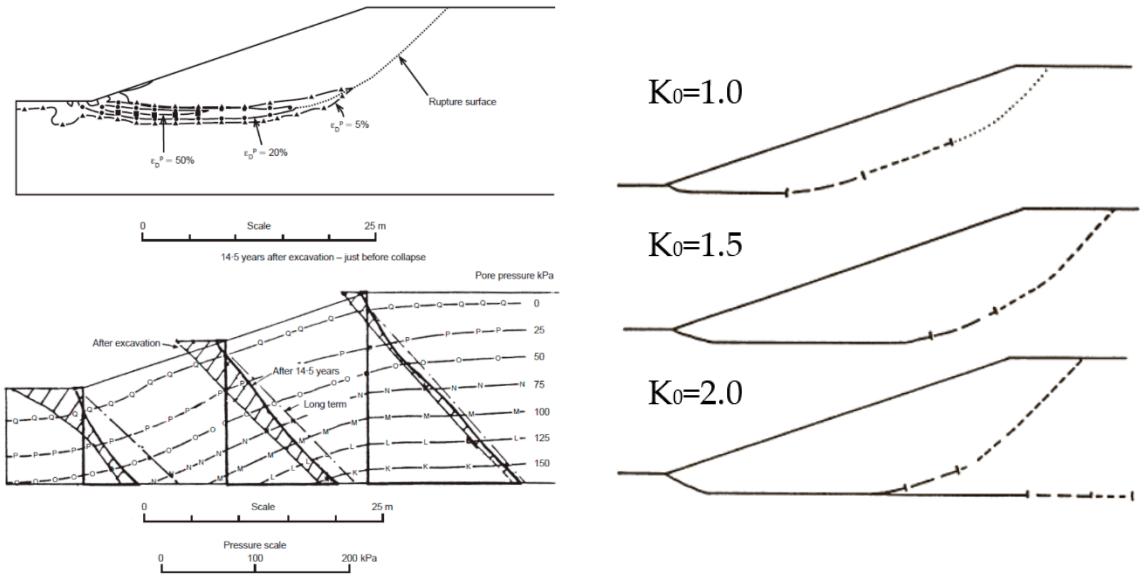

(**a**) (**b**)

Figure 12. Coupled hydro-mechanical numerical modelling of the effects with time of the slope excavation in London clay: results of numerical FE analyses with negative hardening (**a**) and effect of K_0 on the shape of the predicted shear band ((**b**); [5]).

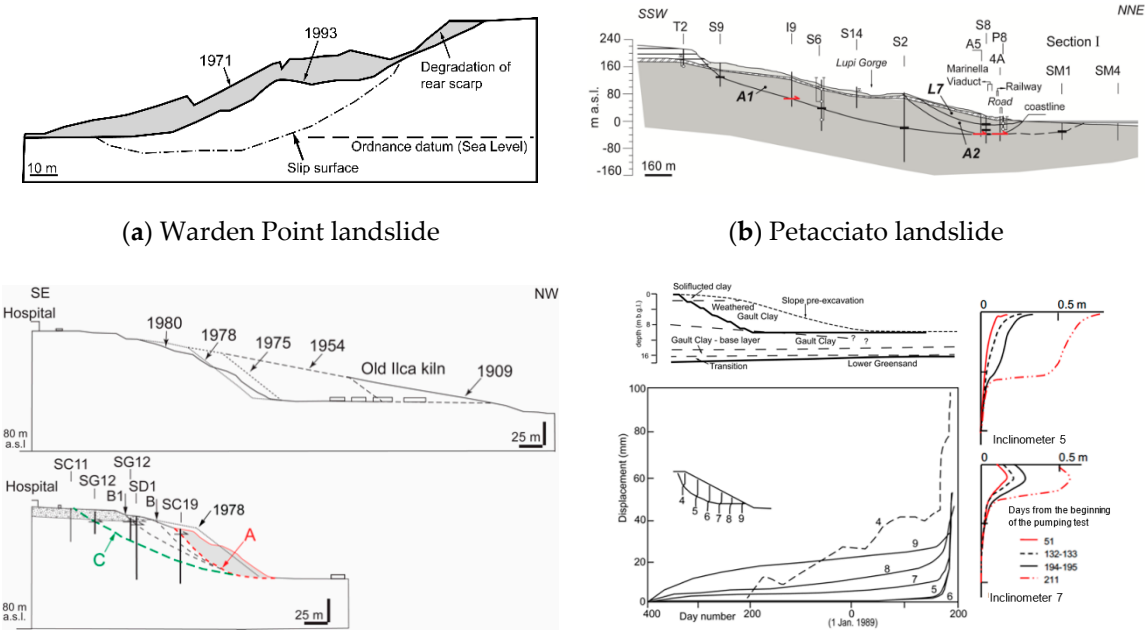

(**c**) Lucera landslide (**d**) Selborne landslide

Figure 13. Some rototranslational landslides in stiff clays (class 1 in Figure 11; Table 3; modified from [79]—(**a**) Warden Point landslide, [80]—(**b**) Petacciato landslide, [38]—(**c**) Lucera landslide, [83]—(**d**) Selborne landslide).

For the landslide class 1, after either natural or anthropic excavation, the slope is firstly involved in a rotational failure mechanism. The numerical modelling performed in the stage III analyses (e.g., [5,38,67,86]) demonstrated how the excavation process triggers the creation of a shear band at the toe of the slope, which propagates upslope over time (Figures 12 and 13). The morphology of the shear band and the duration of the progressive failure are controlled by various factors, such as: (1) the slope

gradient due to the excavation (i.e., by the value of the mobilized shear stresses); (2) the value of the clay coefficient of permeability and of its volumetric stiffness modulus (hence, of the consolidation coefficient); (3) the hardening law of the clay; and (4) the plastic flow of the elasto-plastic constitutive law. In general, even for homogeneous clay slopes, the modelling shows that the morphology of the shear band is not necessarily circular, but can be composite (Figure 11). Potts et al. [5] and, recently, Tagarelli V. and Cotecchia F. [67], highlighted the incidence of the earth pressure coefficient at rest, K_0, of the clay on the morphology of the landslide body, showing that this deepens with the increase of K_0. Moreover, when negative hardening becomes important, the bifurcation of the shear band occurs for high K_0, with the activation of multiple rototranslational mechanisms (Figure 12b).

Reactivated rototranslational landslides, such as the Petacciato (Figure 13b) and Tolve landslides (Figure 7), are still part of class 1. In this case, however, the GHM study deals with the re-activation causes, which generally differ from first-failure ones. Accordingly, for the deep-seated Petacciato paleo-landslide, the current activity is due to the presence of very high piezometric heads at large depth, near the pre-existing shear band, as recognized during stage I studies (Figure 13b; [10,80]) and predicted through stage III modelling. In particular, the fissuring of the deep clay part of the pre-existing shear band determines the occurrence of the deep slope portions of higher coefficient of permeability (Table 3). Such a feature eases the presence of high hydraulic heads at large depth, which predispose the landslide to re-activation.

Class 2 landslides (Figure 11) typically involve highly sensitive clays, such as quick clays [45,89–95], which are either lateral spreads (Figure 11 and box 2 in Figure 2) or flowslides (Figure 11). The slope soils are generally glacial-marine clays characterized by high sensitivity S_t > 20–30 [96,97], which are mainly located in Northern Europe and North America (Canada, Finland, Norway, Russia, Sweden and Alaska), where they outcrop below coarse-grained moraine deposits and are overlain by either a dried fissured crust or silty-sandy soil strata [98]. The complex landslide mechanism is controlled by the peculiar hydro-mechanical properties of the quick clays, which, due to their high sensitivity, are extremely fragile under shearing, to such an extent as to become a slurry by small shear strains. In particular, in the case of the flowslides (Figure 11), the initial failure develops as a rotational landslide, and is followed by a rapid onset of retrogressive rotational landsliding, as the outcome of the progression of failure upslope, in undrained conditions [99,100]. While advancing, the clay forming the rotational landslide bodies liquefies and flows downstream rapidly. The onset of the downstream clay flow may occur from a few hours (landslide events of Saint-Alban in 1894 and Saint-Thuribe in 1898) to a few days (landslide events of Kenogami in 1924, Saint-Joachim-de-Tourelle in 1963, Saint-Jean-Vianney in 1971, Longue-Rive in 2005) after the activation of the first rotational failure. In contrast, lateral spreads are characterized by extremely rapid horizontal translational movements of blocks of sensitive clay, with a horst and graben structure, moving on a layer of remolded clay (Figure 11; [16,42,77,93]). The extremely fragile mechanical behavior of such materials makes the triggering cause potentially even a small perturbation of the slope system; in particular, both human activity, such as overloading or excavation, and nature itself (e.g., river erosion, natural evolution of the morphology, or earthquakes) can represent a triggering cause of a landslide process in such a context. The areas involved in such landslide mechanisms are large (>1 ha; [74,95]).

Table 4a provides a summary of the GHM factors applying to some flowslides and lateral spreads occurred in Québec from 1840 to 2012. The Saint-Jude flowslide, whose landslide factors are reported in Table 4b, was activated with multiple retrogressive rotational failure in a river bank (Figure 14a; [74,95]). Thereafter, the runout of the landslide bodies across the river occurred as lateral spread. The phenomenological evolution of the landslide process, which lasted only a few minutes, was modelled through numerical analyses performed by means of the PFEM code (particle finite element method; [101]; Figure 14b), within which the Lagrangian formulation of FEM coexists with the particle approach, implementing a hardening elasto-visco-plastic model, which allows for to high fragility.

Class 3 landslides correspond to the compound landslide mechanism (Figure 11) involving slopes made up of stratified sedimentary successions, where weaker layers are interbedded with more

resistant ones. If the bedding planes are dipping in the same direction of the slope and are less inclined than the sloping angle, the progressive failure advances primarily in the weaker layers, as observed in the field and shown in the numerical modelling (Phase I and III in Figure 5) of various case studies. The Vajont landslide (PN) and the Timpone landslide (Senise, PZ) are two such literature case studies.

Table 4. Class 2 (Figure 11): summary of the geotechnical parameters (**a**) of the quick clays of some Canadian landslides [102] and landslide factors (**b**) of the Saint Jude flowslide-spread [74,101]; Key: PI—average values of the plastic index, LI—minimum values of the liquidity index, S_u—minimum values of the undrained shear strength measured with the Swedish cone, S_t—sensitivity measured with the Swedish cone, OCR—overconsolidation ratio, CF—clay fraction.

Property	**Flowslide**	**Lateral Spread**		**Landslide Factors**	**Saint-Jude [74,101]**
PI	1–47%	3–46%		Formation	CSC
LI	1.5–16.5	1.3–5.1	Geological	Tectonic structures	
S_u	0.08–0.8 kPa	0.08–1.3 kPa		First-time failure	Current
S_t	10–1890	12–1500		Classification	C_{so}
OCR	1.1–1.2	1.1–7.9		Grain-size data	CF = 65%
CF	13–88%	27–88%		Index properties	IP = 30%
			Geotechnical	Shear strength parameters	S_u = 25–65 kPa; c' = 8 kPa ϕ' = 35°
				Sensitivity	40–80
				Permeability coefficient	9×10^{-10} m/s
			Piezometric	Piezometric levelsat medium depth	Upslope: −2 m below g.l. Downslope: +4 m below g.l.

(CSC) Champlain Sea Clay, (C_{so}) slightly overconsolidated clay, (g.l.) ground level.

Table 5 reports the landslide factors for the Timpone slope, where the Aliano sands outcrop. This geological formation is represented by sands interbedding either gravel or clay layers. The latter, mostly of centimetric thickness, tend to increase with depth [103–105] and are formed of medium-high plasticity clay, exhibiting negative hardening with shearing. Following an excavation at the slope toe, the failure progressed over time due to the shear strain localization in one or more of the clay layers, leading to the activation of a translational sliding mechanism. The rate of movement of the Timpone landslide was high (maximum velocity of 12.5 mm/s). Troncone et al. [72,106] verified the phenomenological interpretation through nonlocal finite element modelling (using Tochnog) under both two-dimensional and three-dimensional conditions (Figure 15). At Vajont, failure progressed over time with shear strain localization in one or more of the clay layers interbedded within calcareous strata, due to the rise in piezometric head; the latter was caused by the submersion of the slope during the filling of the artificial lake confined by the Vajont dam.

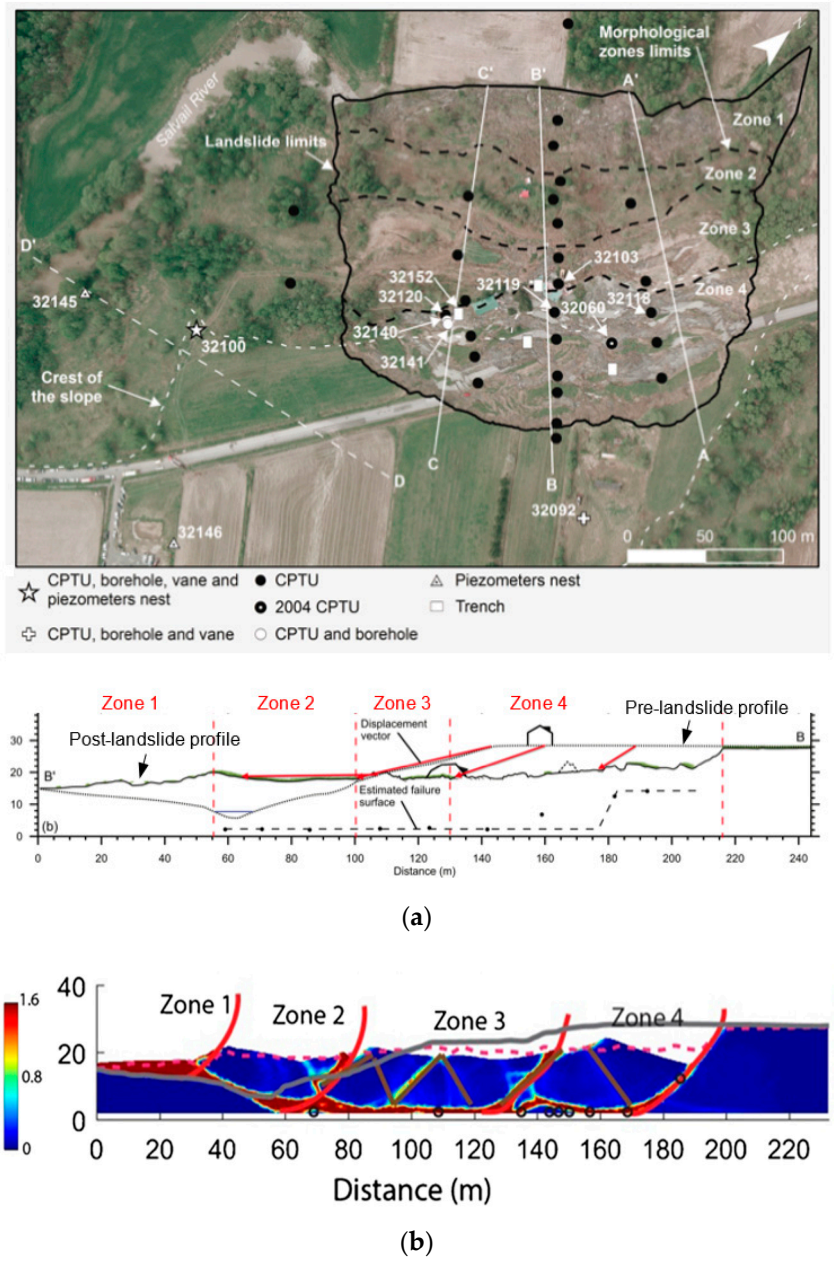

Figure 14. Saint-Jude landslide: (**a**) map and section (Locat et al., 2017); (**b**) Equivalent shear strain field after 87 s (PFEM code; Zhang et al., 2019).

Class 4 landslides are represented by the earthflows [42] and mudslides [15]; see Figure 2 (box 4) and Figure 11. Several earthflow case studies are reported in the literature for Italian sites [12,107–116] and provide the values of the landslide factors, as well as the features of the earthflow kinematics. In particular, Figure 16 shows a morphological map of some of the Italian earthflows reviewed using the present GHM characterization: Vadoncello (Senerchia, AV; [117]), Serrone (Motta Montecorvino, FG; [118]), Costa della Gaveta (PZ; [114,119,120]), Montaguto (BN; [121,122]), Brindisi di Montagna (PZ; [123–125]), Masseria Marino (AV; [108,113,126,127]). The corresponding landslide factor values are reported in Table 6.

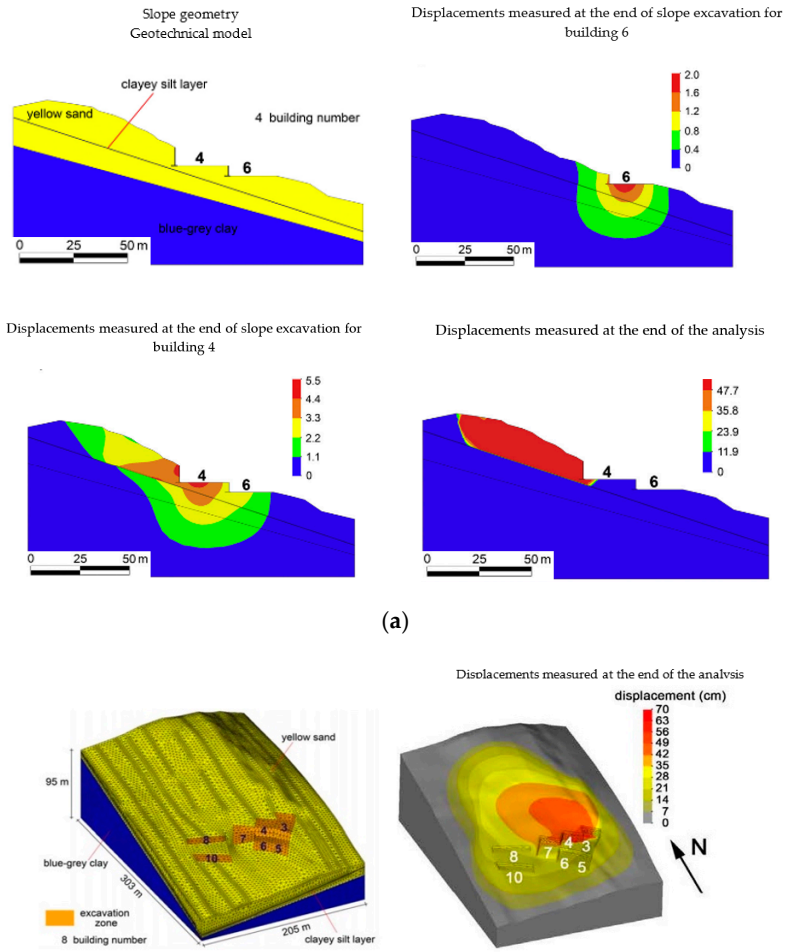

Figure 15. Timpone landslide: finite element numerical modelling performed by means of Tochnog code—2D ((**a**); [72]) and 3D analyses ((**b**); [73]).

Table 5. Landslide factors of the Timpone landslide (class 3; Figure 11; [103,104]); Key: MF—silt fraction, SF—sand fraction, for the other acronyms referring to Table 3.

Landslide Factors		**Timpone [103,104]**
Geological	Formation	Aliano Sands
	Tectonic structures	
	First-time failure	Current
Geotechnical	Classification	(a) Silty sands (b) Silty clays
	Grain-size data	(a) CF = 3%, MF = 23%, SF = 80% (b) CF = 50%, MF = 43%, SF = 11%
	Index properties	(b) PI = 26%, A = 0.54
	Shear strength parameters	(a) c'_p = 50–120 kPa ϕ'_p = 42°; ϕ'_r = 34° (b) c'_p = 70 kPa ϕ'_p = 24°; ϕ'_r = 13°
Piezometric	Water table	Slope involved in landsliding: no groundwater immediately downstream the landslide: water table at 23 m below g.l.

Table 6. Landslide factors of some landslide mechanisms belonging to class 4 (Figure 11; [108,113,114,116–118,122,123,126–129]); for the geotechnical parameters referring to Tables 3 and 5.

Landslide Factors		Vadoncello [117]	Serrone [118]	Costa della Gaveta [114,119,120]	Montaguto [121,122]	Brindisi di Montagna [123–125]	Masseria Marino [108,113,126,127]
Geological	Formation	VC	FAEc—RF	VcC	FAE—VS	RF—VC	VcC
	Tectonic structures			Fault along the channel		Fault along the contact beteween RF and VC	
	First-time failure	Current	Current		Current		Current
	Reactivated failure	Current	Current	Current	Current	Current	Current
Geotechnical	Classification	C_{hFS}	A_{imF}	C_S with rock blocks	FAE: limestone and clay	C_{mFS} with rock blocks	C_S with rock blocks
	Grain-size data	CF = 52%	FAEc−CF = 60% RF−CF = 50%	CF = 38%	FAE CF + MF = 70%	RF/VC CF = 38%	CF = 40%
	Index properties	PI = 38%, A = 0.4–0.8	FAEc: PI = 42%, A = 0.7 RF: PI = 19% A = 0.4	PI = 35%	FAE PI = 35%	RF/VC PI = 51%	PI = 28% A = 0.7
	Shear strength parameters	c'_p = 0 kPa ϕ'_p = 19° ϕ'_r = 5°	FAEc: c'_p = 0 kPa ϕ'_p = 21° ϕ'_r = 8.2° RF c'_p = 10 kPa ϕ'_p = 23° ϕ'_r = 9°	c'_p = 50 kPa ϕ'_p = 14° ϕ'_r = 10°	FAE c' = 0 kPa ϕ' = 20°	RF: c'_p = 8–17 kPa ϕ'_p = 16–25°, ϕ'_r = 5.3° VC: c'_p = 8–17 kPa ϕ'_p = 16–25°	c'_p = 8 kPa ϕ'_p = 25° ϕ'_r = 11.4°
	Permeability coefficient (m/s)		Lab.: FAEc: 1×10^{-9} RF: 5×10^{-9}–3×10^{-11} Field: 5×10^{-9}–10^{-8}	10^{-9}	FAE Field: 10^{-5}–10^{-7}		9×10^{-10}
Piezometric	Piezometric levels (m g.l.)	−7/−9 (body) −12.8/−15 (substratum)	−2/−3 (water table)	−1/−5 (body)	−10/+20 (water table in the source area)	−1.7/−2.2 m g.l. (water table)	+3/−9 m g.l. (body and substratum)

(VS) Villamaina Synthem; FAE) Faeto Flysch (FAEc: clayey member), (VC) Variegated Clays; (VcC) Varicoloured Clays; (RF) Red Flysch; (C_{hFS}) highly fissured and scaly clays; (C_{imF}) highly to medium fissured clays; (C_S) scaly clays; (C_{mFS}) medium fissured to scaly clays.

As shown in Figure 16, the detachment area of the landslide mass, where failure is triggered, may extend through one or more source areas, from which the mass propagates through a channel experiencing major straining, reaching a distant accumulation area downslope. The morphological features of these landslides are largely controlled by the soil hydro-mechanical properties and the slope orography. Based upon the data in Table 6, earthflows often appear to involve slopes where structurally complex [130], clayey formations outcrop. These are sedimentary successions of fine soils, sedimented in pre-orogenic marine basins and subsequently involved in orogenetic processes. At the locations of the case studies in Table 6, these successions are chaotic and jointed as a consequence of an intense tectonic history, so that fractured rock blocks float in an intensely disturbed and highly fissured plastic clay matrix which controls the overall slope behavior. In addition, faults and overthrusts may affect the slopes, determining the presence of localized weaker portions across the slope [131–135]. Irrespective of the geological and geo-structural history, the clays in these slopes exhibit the behavior of overconsolidated clays, with yield stress ratios in compression, i.e., YSR ≥ 3 [134]. Especially for the scaly clays (Variegated Clays, Varicoloured Clays or Red Flysch), extensive experimental studies have provided evidence of very low values of peak strength parameters, c'_p e ϕ'_p [134,136–140], as reported in Table 6. The corresponding residual friction angles, ϕ'_r, are of the order of 5–10°. Furthermore, for slopes made of fissured clays, the saturated permeability coefficient, K_s [141], is generally higher than that of intact clay (see for instance Table 3). Furthermore, K_s is even higher at the slope scale (Table 6), given the interbedding of both coarser strata and floating fractured rock blocks. In addition, the permeability of the runout material in both the channel and the accumulation area (generally referred to as debris, i.e., clayey matrices incorporating rock fragments) is generally higher than that of the in situ soil [142,143]. The relatively high permeability values and the hydraulic boundary conditions of the slope (Table 6) generally cause the piezometric heads to be significantly high, especially in the runout landslide portion, where the water table is often about the ground level. Therefore, the low strength of the clays dominating the slope hydro-mechanic behavior, along with the seepage regime across the slope, are both factors predisposing the slope to landslides.

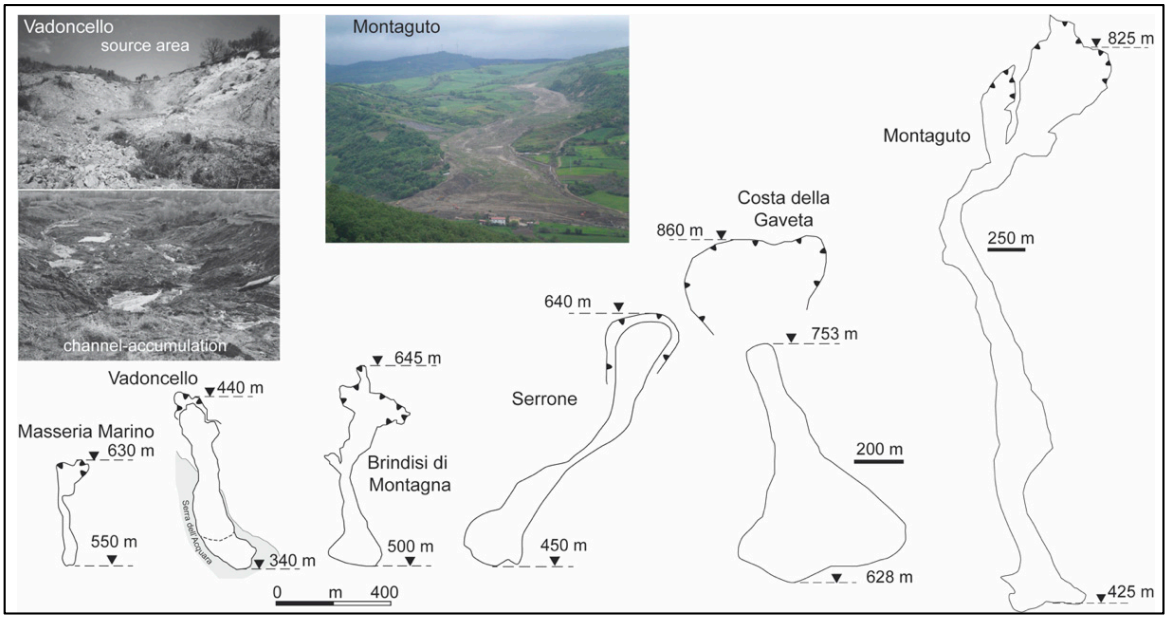

Figure 16. Some earthflows/mudslides (class 4; Figure 11 and Table 6; modified from [116,117,121]).

As is the case at the Serrone and Vadoncello sites (Table 6; Figure 16), the earthflow mechanism can result from the onset of a retrogressive rototranslational sliding in the source area, the location of clayey flysch and the runout of the landslide mass downslope. In the case of the Serrone slope, temporal geomorphological analyses (through the stereoscopic study of aerial photos) have suggested

that the failure in the source area was an effect of an unloading process at mid-slope, determined by the movement of a pre-existing rototranslational landslide in the base portion of the slope, activated by toe river erosion [118]. Such an old landslide body is overlain by the runout of the earthflow. In the Vadoncello slope, a similar process took place over time, given the existence of a pre-existing ancient landslide in the base portion of the slope. In this case, however, such a landslide body was reactivated by the movement in its toe area of another active landslide body (Serra dell'Acquara landslide), of which the Vadoncello landslide is subsidiary [41,117]. Therefore, temporal analyses showed that in both slopes, the toe of the rototraslational landslide in the source area corresponds to the main scarp of an older landslide, lying downslope, which underlies the present earthflow channel and accumulation materials. Such an interpretation of the earthflow mechanism was confirmed, for the Vadoncello case study, by the results of FEM modelling, as discussed by Cotecchia et al. [41,144]. For both case studies, the depth of the slope failure in the source area was from medium to large. Moreover, the earthflow displacement rates were observed to increase, reaching meters/day, either when failure was reactivated in the source area, or after intense and long duration rainfall events, determining the increase of the pore water pressures within the channel material and in the accumulation zone.

For the Costa della Gaveta earthflow (Table 6; Figure 16), the multisource area is located within an ancient landslide basin, including several subsidiary bodies, according to numerous accurate field surveys and temporal geomorphological analyses (Figure 5; [114,119]). This earthflow is characterized by a short channel area and involves tectonized clays, where rock blocks are dispersed within a scaly matrix. In the channel area, the sliding surface occurs at a depth of about 10 m, while the thickness of the landslide body in the accumulation area is greater (38 m). According to the inclinometric monitoring data, the earthflow body moves through the transversal sections at a constant, very low to extremely low mass rate. The river erosion of the landslide toe contributes to the activity of the landslide [114,119]; in addition, recent 3D modelling of the seepage regime in the slope [128], validated by piezometric monitoring, showed that the seasonal rainfall infiltration also influences the landslide activity.

The Masseria Marino and Brindisi di Montagna landslides (Table 6; Figure 16) are representative of many other earthflows occurring in the Basento Valley [110]. The interpretation of the Masseria Marino earthflow mechanism was based on both phenomenological (stage I) and numerical (stage III) analyses, supported by accurate monitoring of the displacements, both at ground level and at depth, and of the piezometric levels [108,113,127]. This earthflow involves, again, intensely fissured clays, which result largely from the runout of a wide landslide in the upslope area; the latter is also characterized by an intermittent retrogressive activity. The runout material moving downslope influences the kinematics of the channel body, whose displacement rates vary from a few mm/year to 12 cm/day [110,113,116]. Moreover, the channel movements appear also to be connected to the increase in the pore water pressures related to the seasonal rainfall infiltration. According to Pellegrino et al. [145], the activity of the earthflow is controlled by a combination of processes, both drained and undrained, i.e., the impact of the runout material coming from the upslope area and rainfall infiltration.

The interpretation of the Brindisi di Montagna earthflow mechanism (Table 6; Figure 16) is derived from the stage I, II and III analyses performed by various authors [123,125,146]. Again, the earthflow materials derive from the runout of an ancient and wide rotational landslide upslope in a source area location of important tectonic displacements due to the activity of a fault. Therefore, the clayey soils in the source are fissured and have a very chaotic structure, and the earthflow body is largely made of scaly clays, including disarranged rock blocks. As a whole, the earthflow activity is intermittent, characterized by variable displacement rates, from a few mm/year to 1 m per day. The activity relates to both the piezometric level fluctuations, resulting from the rainfall infiltration, and the undrained loading determined by the runout material moving from the source area, where the top landslide reactivation occurs [125].

The evolution of the Montaguto earthflow [121,122,147] was inferred from analyses conducted according to all the three stages of the diagnostic methodology in Figure 5, including extensive topographic (LIDAR, robotic total stations, GBInSAR), inclinometric and piezometric monitoring.

The earthflow body is made of remolded clay with rock fragments, coming from the Faeto Flysch Formation which outcrops in the source area. The substrate, on which the earthflow moves (channel and accumulation area), consists of clayey marls and fine sands belonging to the Villamaina Synthem. In 1954, the source area of the earthflow was affected by multiple landslide events, the toe of which was at midslope. Recently (2005–2006; 2010), according to Lollino et al. [122,147], on the basis of monitoring data and numerical modelling, the reactivation of movements was shown to be due to consolidation processes following the undrained loading caused by the runout masses from the source area.

In summary, all the earthflow case studies discussed above provide evidence of similarities in the values of the main landslide factors and in the landslide mechanism. The disturbed and heterogeneous features of the soils involved in the earthflowing, generally disturbed and fissured clays of low shear strength, including floating rock blocks, represent a factor predisposing the slope to landslides. At the same time, the fissuring of the clays and the presence of either fractured rocky strata or coarse soil strata provide the slope with an overall permeability that is higher than that applying to clay slopes, which allows for significant water infiltration, fed either by the rainfall or upslope aquifers, which are the hydraulic boundary conditions of the slope. Such infiltration determines high piezometric heads up to medium depths, which represent an additional factor predisposing the slope to landslides. In this hydro-mechanical context, earthflows result from the runout of landslide bodies activated in the source areas, which is generally the steeper part of the slope, and often includes a higher content of either rocky or coarse soil strata. In the channel portion of the earthflow, the landslide body is from superficial to medium deep, but becomes deeper in the accumulation area, and in both areas, the earthflow is not necessarily formed solely of the runout material, but often also involves the top strata of the in situ formations. The prolonged activity of the earthflows appears to result in: (i) the mobilization of the channel material, often involving the underlying in situ clays; (ii) the retrogression of the landslide in the source area; (iii) the activity of the original, pre-existing landslide in the toe area, where present. This activity may be related to: (1) the undrained loading determined by the impact of landslide masses coming from the source area, and the following consolidation processes; (2) excursions of the piezometric heads in the channel area and in the accumulation zone, due to rainfall infiltration; (3) the lateral unloading in the toe area. The contribution of creep to the earthflow slow movements cannot be excluded.

Class 5 landslides include mainly mixtilinear sliding processes (Figure 11) in slopes whose hydro-mechanical setup is still quite complex, but slightly less chaotic than those of the typical locations of earthflows. The slopes are still composed of clayey flysch, in which the clays are of high plasticity and often fissured, and interbed rock blocks or isolated coarser soil layers. The landslides, however, are rototranslational, of medium to high depth, with the toe generally at the base of the valley. In these slopes, the more permeable layers (fissured clays and embedded fractured rock blocks) allow for a high rainfall water infiltration into the slope, which causes an increase of the pore water pressures up to significant depths. Examples of landslide mechanisms of such a typology (Figure 11) are the landslides (Table 7): Fontana Monte (Volturino, FG; [147–149], Pisciolo [40,41] and Pianello (Bovino, FG, [150]). The geomorphological maps and sections of the latter two case studies, deduced from extensive phenomenological studies, are shown in Figures 6 and 17, respectively. Table 7 shows the synthetic characterization of the landslide factors which are representative for many other similar landslides within the south-eastern Apennines [11,40,41,59]. As can be deduced from Table 7, the clays involved in the sliding process are of medium-high plasticity and have relatively low strength parameters, despite their overconsolidation degree [41].

Table 7. Landslide factors for deep rototranslational landslides (class 5; Figure 11; [40,150]); for the geotechnical parameters referring to Tables 3 and 5.

Landslide Factors		Pisciolo [40,41]	Pianello [150]
Geological	Formation	PD	FAEa
	Tectonic structures	Fault and fold	Overthrust
	First-time failure	Current Current	Before the '50 s Current
Geotechnical	Classification	C_{imFoc}	C_{Foc}
	Grain-size data	CF = 49% MF = 45% SF = 6%	CF = 45% MF = 27% SF = 14%
	Index properties	PI = 40% A = 0.85	PI = 44% A = 0.9
	Shear strength parameters	c'_p = 20 kPa ϕ'_p = 18° ϕ'_r = 10°	c'_p = 0–25 kPa ϕ'_p = 13°–26° ϕ'_r = 8.5°
	Permeability coefficient (m/s)	Lab: 10^{-9}–10^{-10} Field: 10^{-8}–10^{-9}	Lab: 10^{-9}–10^{-10}
Piezometric	Piezometric levels from shallow to large depth (m g.l.)	−2/−3	−2/−3

(PD) Paola Doce Clays; (FAE) Faeto Flysch (FAEc clayey member); (C_{imFoc}) intensely to medium fissured, highly overconsolidated clays; (C_{Foc}) fissured and highly overconsolidated clay.

Moreover, the permeability coefficient at the slope scale, K_s, can exceed 10^{-9} m/s up to significant depths (Table 7). As previously noted, although the main slope lithotype is clay, the relatively high permeability at the site scale, combined with the hydraulic boundary conditions, provides the slope with piezometric levels reaching about 2–4 m below ground level, even for the deep strata. Such piezometric heads are an internal cause of the medium depth or deep rototranslational landslide mechanism of the type in Figure 11 (Figure 2, box 5), despite the quite low average slope angles (12°; Figures 6 and 17). However, the locations of slopes of this landslide class, despite being formed of materials similar to those involved in the earthflows discussed above (Figure 16), are characterized by an orography and geo-structural settings which are less chaotic than those involved in earthflows. In addition, the presence of clays of low strength parameters down to great depths makes these landslide mechanisms deeper, involving the whole slope down to the bottom of the valley. FEM modelling has also shown the extent to which valley excavation determined by river erosion over geological time periods can give rise to the onset of failure progression in these slopes, from the toe upwards. At present, the current activity of these landslides is often related to slope-vegetation-atmosphere interactions [11,40,64–66]; Figures 7, 9 and 10).

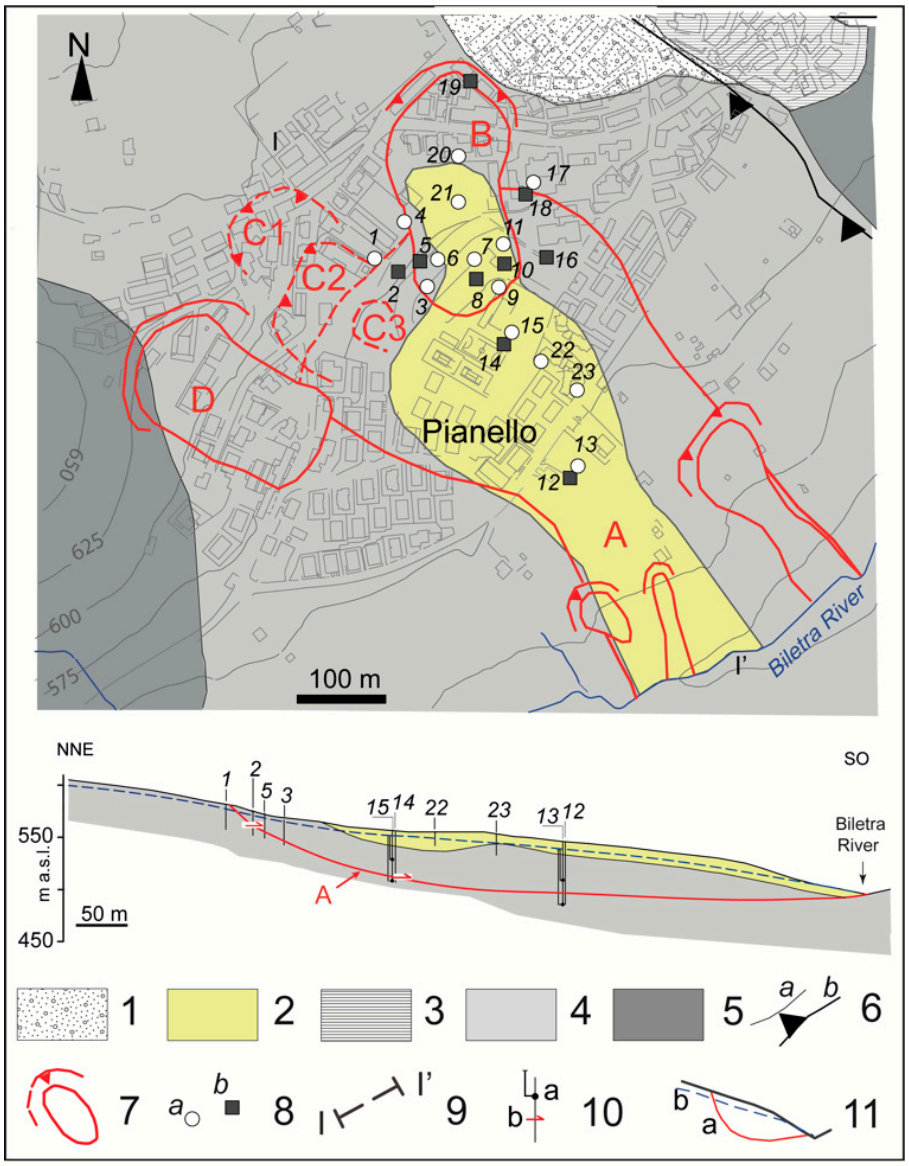

Figure 17. Pianello landslide (class 5 in Figure 11; Table 7): (1) debris; (2) remoulded clays; (3) Bovino Synthem; (4) Faeto Flysch (limestone member); (5) Faeto Flysch (clayey member); (6) stratigraphic contact (a) and over-thrust (b); (7) landslide crown (a) and body (b); (8) borehole with piezometers (a), borehole with inclinometer (b); (9) line of section; (10) piezometer cell with corresponding hydraulic heads (a) and inclinometer shear bending (**b**); (11) labelled landslide portions: crown (a), slip surface (b).

Debris-flow, debris-avalanche and debris/sand flowslides ([42]; box 6 in Figures 2 and 11) are part of the 6th landslide class examined in this paper. They are generally triggered by more or less critical rainfall events, which mobilize coarse to loamy soil covers, propagating downslope as rapid flows. In the following paragraphs, we will refer to this class with the term "flow". These flows occur in different geological contexts, where pyroclastic soils (Central America: [151]; New Zealand: [44,129,152–161]), residual soils (Hong Kong: [162]; Japan: [163]) or colluvial soils (Brazil: [164]; Hong Kong: [165]) overlay rock bedrocks. In Campania, Italy, these landslides are very common, where pyroclastic deposits outcrop on the fractured limestones of the Apennine platform. The flows of reference in the analysis occur at Mt. Lattari (1997), Mt. Pizzo D'Alvano and San Felice a Cancello (1998), Cervinara (1999), Nocera Inferiore (2005) and Ischia (2006). In some cases, these flows involve pyroclastic soils lying on flysch outcroppings within the Apennines (event 2005 in the area of Mt. Le Croci-Monte Termito). Table 8 summarizes the landslide factors of some of the cited case studies: Cervinara, Monte Pizzo

d'Alvano (Figure 18), Monte Albino and Bosco de' Preti flows. For all these flows, the pyroclastic cover, on average from 2 m to 4.5 m thick, consists of ashes interbedding pumices [160,166,167]. As a result of accurate field surveys, geotechnical monitoring and numerical modelling, these flows result from the onset of failure within the pyroclastic cover (mostly a sliding process in the source area), followed by the propagation of the debris downhill. Usually, the mass travels rapidly downslope, through a channel, reaching distances of several kilometers from the source area [42]. Generally, the flows involve additional saturated soil all along the runout path, which adds to that coming from the source area [42].

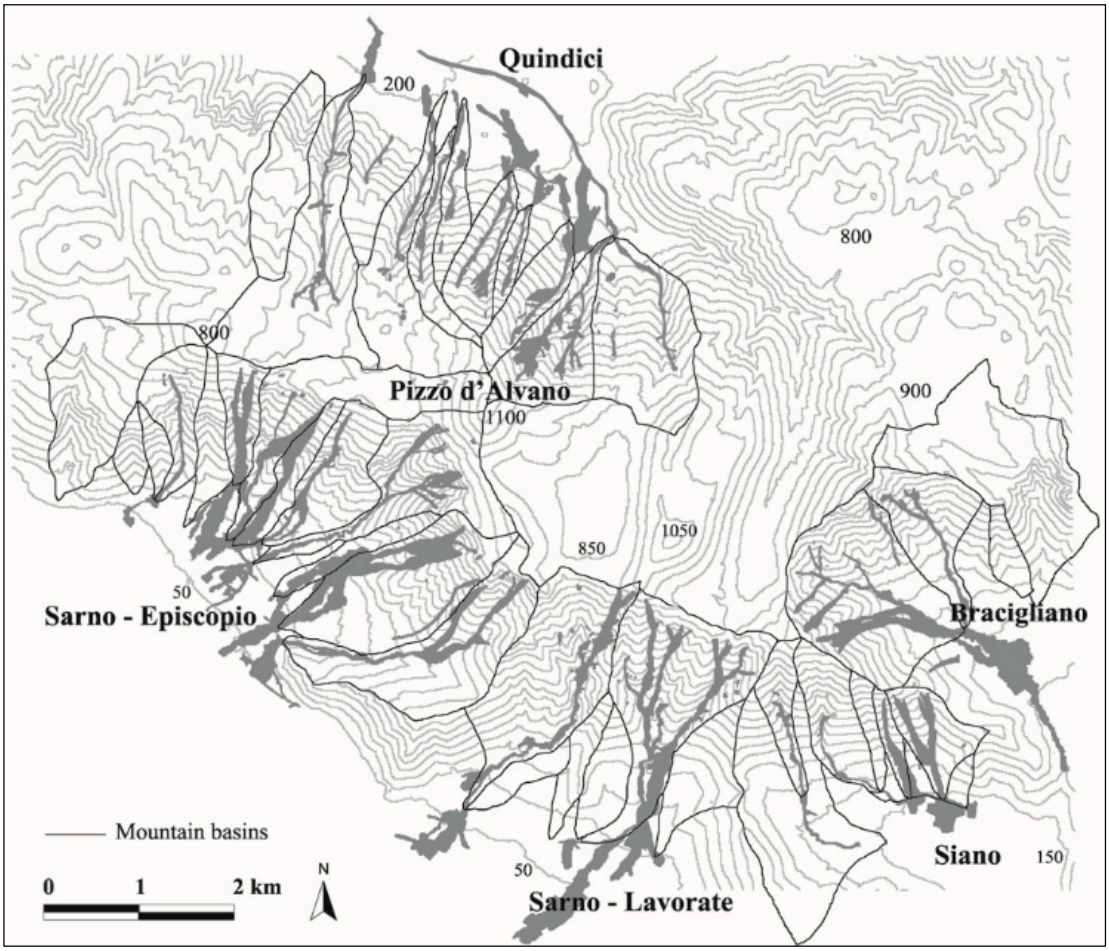

Figure 18. Debris flows involving the pyroclastic deposits lying on the limestone bedrock at Pizzo d'Alvano during the 1998 event (class 6; Figure 11 and Table 8; [168]).

Table 8. Landslide factors of flows (class 6, Figure 11; [157,159–161,166–173]); Key: GF = gravel fraction; γs = specific weight, γd = volume unit weight, n = porosity, for the other geotechnical parameters referring to Tables 3 and 5.

Landslide Factors		Cervinara [157,167,169–171]	Mt. Pizzo d'Alvano [166,168,172]	Monte Albino [161,173]	Bosco dei Preti [160]
Geological	Cover	Fall pyroclastites	Fall pyroclastites	Fall pyroclastites	Fall pyroclastites
	bedrock	limestone	limestone	limestone	flysch
	Tectonic structures		Normal fault system	Normal fault system	
Geotechnical	Classification	(a) coarse pumices (b) volcanic ash (c) fine pumices and ash (d) weathered ash	(a) coarse volcanic ash (b) pumices (c) fine volcanic ash	(a) coarse volcanic ash (b) pumices (c) fine volcanic ash	Ash Pumices Ash
	Grain-size data (%)	(a) MF = 2, SF = 52, GF = 46 (b) CF = 6, MF = 10, SF = 80, GF = 4 (c) CF = 1, MF = 8, SF = 58, GF = 33 (d) CF = 8, MF = 27, SF = 60, GF = 5	(a) CF = 2, MF = 28, SF = 57, GF = 13 (b) MF = 11, SF = 43, GF = 46 (c) CF = 5, MF = 45, SF = 46, GF = 4	(a) CF = 2, MF = 32, SF = 44, GF = 21 (b) MF = 1, SF = 24, GF = 75 (c) CF = 18, MF = 45, SF = 34, GF = 3	Ash CF = 8%, MF = 34%, SF = 48%, GF = 10%
	Physical properties	(a) γ_s = 25 kN/m^3, γ_d = 12 kN/m^3, n = 0.52 (b) γ_s = 26 kN/m^3, γ_d = 8 kN/m^3, n = 0.69 (c) γ_s = 26 kN/m^3, γ_d = 13 kN/m^3, n = 0.50 (d) γ_s = 26 kN/m^3, γ_d = 12 kN/m^3, n = 0.54	(a) γ_s = 25 kN/m^3, γ_d = 9 kN/m^3, n = 0.61 (b) γ_s = 13 kN/m^3, γ_d = 6.2 kN/m^3, n = 0.69 (c) γ_s = 24 kN/m^3, γ_d = 8 kN/m^3 n = 0.69	(a) γ_s = 26 kN/m^3, γ_d = 8.6 kN/m^3, n = 0.67 (b) γ_s = 13 kN/m^3, γ_d = 6 kN/m^3, n = 0.69 (c) γ_s = 25.7 kN/m^3, γ_d = 8.8 kN/m^3, n = 0.67	Ash γ_s = 12 kN/m^3, γ_d = 7.1 kN/m^3, n = 0.71
	Shear strength parameters	Saturated conditions: (b) c′ = 0 kPa ϕ′ = 38° (d) c′ = 11 kPa ϕ′ = 31°	Saturated conditions: (a) c′ = 0–3 kPa, ϕ′ = 36–41° (b) c′ = 0 kPa, ϕ′ = 37° (c) c′ = 0–3 kPa, ϕ′ = 30–35°	Saturated conditions: (a) c′ = 5 kPa, ϕ′ = 37° (b) c′ = 0 kPa, ϕ′ = 37° (c) c′ = 6 kPa, ϕ′ = 31°	Saturated Conditions for ash: c′ = 0 kPa, ϕ′ = 37°

Table 8. *Cont.*

Landslide Factors		Cervinara [157,167,169–171]	Mt. Pizzo d'Alvano [166,168,172]	Monte Albino [161,173]	Bosco dei Preti [160]
	Permeability coefficient (m/s)	(a) $\times 10^{-6}$–6×10^{-6} (b) $\times 10^{-7}$–5.5×10^{-7} (c) 5.0×10^{-6}–9×10^{-7} (d) 8.5×10^{-8}–6×10^{-7}	(a) 10^{-5} (b) 10^{-4} (c) 10^{-6}		1.2×10^{-6}
Piezometric	Suction	Winter: 2 kPa (z < 2.5 m g.l.) 15 kPa (z > 2.5 m g.l.) Summer: 30–80 kPa	z <1 m g.l. Winter: 10 kPa, Summer: 35 kPa 1< z <4 m g.l. Late autumn: 30 kPa, Summer: 37 kPa	z = 0.2–0.4 m g.l. Winter: 10 kPa	

In general, the reduction of the soil suction within the soil cover is the main triggering factor of flows. Such a reduction may be related to rainfall infiltration. However, several authors have shown that the trigger of flows relates not only to single rainfall event features (i.e., duration and mean intensity), but also to the initial conditions of the soil slope, determined by antecedent precipitations. For instance, the space–temporal variations in matric suction and volumetric water content within a pyroclastic cover were measured at Monteforte Irpino and Cervinara [157,167,169–171]. Consequently, some correlations among the rainfall events, the evapotranspiration rates and the fluctuations of the water level in the underling limestone aquifer were pointed out. In particular, as discussed in Pirone et al. [157], matric suction and volumetric water content in the top part of the soil cover (0.25–0.45 m) can be affected by a single rainfall event, but their temporary fluctuation connected to the rainfall event is relatively small compared to their seasonal fluctuation due to seasonal slope–atmosphere interactions. Seasonal variations in matric suction and volumetric content are well recorded within deeper soils, although their size decreases with depth. On the whole, since the water seepage across the slope is caused by a combination of these processes, their activation has been shown to be highest from December to April.

Cascini et al. [168,172] characterized different features of the flow triggering mechanism in pyroclastic soils covering a carbonate substratum, in relation to the geological, morphological and hydrogeological conditions of the source area, as well as to anthropogenic actions which have affected such areas. Field observations and numerical modelling have suggested that the temporary storage of water in a perched water layer, in the upper part of the fractured and karsified limestone bedrock, may affect the leakage through the soil cover-bedrock interface and influence the soil suctions within the pyroclastic covers, contributing to trigger flows [171,174].

The results of numerical analyses of the seepage regime within the unsaturated pyroclastic cover, influenced by both the underlying perched aquifer and the soil-vegetation-atmosphere interaction, have been implemented either in slope stability analyses conducted with the limit equilibrium method [44,155,157,160,173], or in numerical analyses [44].

Concerning the Pizzo d'Alvano slopes, Cascini et al. [172] showed how different stratigraphic settings and mechanical properties of covers may affect the depth of the sliding mechanism, while Forte et al. [173] demonstrated the influence of topography and stratigraphic settings on the activation of flows in the Monti Lattari area.

With reference to the flows activated along the slopes of Monte Le Croci—Monte Termito, Santo et al. [160] showed, through a numerical analysis of a boundary value problem, how the trigger was predisposed by the infiltration of rain prior to the landslide event, which saturated the cover and raised the water table in the bedrock until it reached the cover. Altogether, the aforementioned models may constitute platforms for the design of early warning systems for risk mitigation at the slope scale.

4. Conclusions

The initial results of the application of the methodology proposed in the paper, which is aimed at deriving a GHM characterization of landslide classes, appear to be promising, leading to successful characterizations through the systematic use of the methodology. Even if the database of reference in the paper, which collected the results of GHM studies of various landslide mechanisms, is limited, it has been shown how the analysis of such a database, through the stage-wise methodology, leads to the assessment of the main features of a landslide's morphology and activity for the six selected landslide classes (Figure 11), as well as of the repetitive hydro-mechanical processes active in the slope for the selected types of landslides, and to the identification of limited ranges of values of the main landslide factors. Such an assessment is expected to improve greatly through the analysis of a larger database and with further insights into the details of each case study, in order to comply more with the complexity of some landslide mechanisms and their variability within each landslide class.

However, the success of the GHM characterization of the landslide classes distinguished in the geomorphological classification of landslides [16] also requires persistence in systematically carrying

out GHM studies of landslides, using so-called stage-wise methodology. Furthermore, the collection and analysis of the results of this type of study, carried out using the methodology discussed herein, may succeed in deriving the GHM characterization of the landslide classes if several researchers cooperate in this type of work.

The initial results presented in this paper nonetheless indicate that the results of the research project being proposed can be of service to practitioners involved in the design of sustainable landslide mitigation measures. Furthermore, they are indicative of the potential long-term value of GHM classification of landslides, which could facilitate much more advanced management of the disasters caused by landslides in several high landslide susceptibility regions around the world.

Author Contributions: All authors have given the same contribution to this article. All authors have read and agreed to the published version of the manuscript.

Funding: This research was funded by the Italian Ministry for Research and University, PRIN 2015 grant (Prot. 201572YTLA).

Acknowledgments: The authors would like to thank Vincenzo Cotecchia and Gregorio Melidoro for the illuminating transfer of knowledge about landsliding, which ever since prompted the recognition of the importance of a geo-hydro-mechanical classification of landslides.

Conflicts of Interest: The authors declare no conflict of interest.

Abbreviations

τ_m	mobilized shear stress
τ_{mf}	soil shear strength
σ_{ij}	components of the stress tensor
δ_{jz}	Kronecker delta
ε_{ij}	components of the strain tensor
ρ_w	water density
k_i	hydraulic conductivity along the i-direction
h	piezometric head
γ	unit weight of the soil
e	void ratio
γ_s	unit weight of the solid particles
γ_d	unit weight of the dry soil
S_r	degree of saturation
χ	Bishop's effective stress parameter
u_a	pore air pressure
u_w	pore water pressure
σ'_{ij}	components of the effective stress tensor
P_l	liquid pressure
P_g	gas pressure
T	temperature
u	displacement tensor
PI	plasticity index
LI	liquidity index
A	activity index
S_u	undrained cohesion
OCR	overconsolidation ratio
c'_p	peak effective cohesion
ϕ'_p	peak effective friction angle
ϕ'_r	residual effective friction angle
CF	clay fraction
MF	silt fraction
SF	sand fraction
GF	gravel fraction

References

1. Froude, M.J.; Petley, D.N. Global fatal landslide occurrence from 2004 to 2016. *Nat. Hazards Earth Syst. Sci.* **2018**, *18*, 2161–2181. [CrossRef]
2. Lin, Q.; Wang, Y. Spatial and temporal analysis of a fatal landslide inventory in China from 1950 to 2016. *Landslides* **2018**, *15*, 2357–2372. [CrossRef]
3. Salvati, P.; Rossi, M.; Bianchi, C.; Guzzetti, F. *Landslide Risk to the Population of Italy and Its Geographical and Temporal Variations*; Chavez, M., Ghil, M., Urrutia-Fucugauchi, J., Eds.; Extreme Events: Observations, Modeling, and Economics, Geophysical Monograph Series; John Wiley & Sons, Inc.: Hoboken, NJ, USA, 2016; pp. 177–194.
4. Wilde, M.; Günther, A.; Reichenbach, P.; Malet, J.; Hervás, J. Pan-European landslide susceptibility mapping: ELSUS Version 2. *J. Maps* **2018**, *14*, 97–104. [CrossRef]
5. Potts, D.M.; Kovacevic, N.; Vaughan, P.R. Delayed collapse of cut slopes in stiff clay. *Géotechnique* **1997**, *47*, 953–982. [CrossRef]
6. Amatruda, G.; Bonnard, C.H.; Castelli, M.; Forlati, F.; Giacomelli, L.; Morelli, M.; Paro, L.; Piana, F.; Pirulli, M.; Polino, R.; et al. *A Key Approach: The IMIRILAND Project Method*; Bonnard, C., Forlati, F., Scavia, C., Eds.; Identification and Mitigation of Large Landslide Risks in Europe, Advances in Risk Assessment, European Commission, Fifth Framework Program; Balkema: London, UK, 2004; pp. 13–44.
7. Lacasse, S.; Nadim, F. Landslide risk assessment and mitigation strategy. In *Landslides—Disaster Risk Reduction*; Springer: Berlin, Germany, 2009; pp. 31–62.
8. Vaciago, G. The SafeLand compendium of landslide risk mitigation measures. In *Landslide Science and Practice: Risk Assessment, Management and Mitigation, Proceedings of the 2nd World Landslide Forum, WLF 2011, Rome, Italy, 3–9 October 2011*; Springer: Berlin/Heidelberg, Germany, 2013; Volume 6, pp. 683–689.
9. Cotecchia, F.; Ferlisi, S.; Santaloia, F.; Vitone, C.; Lollino, P.; Pedone, G.; Bottiglieri, O. La diagnosi del meccanismo di frana nell'analisi del rischio, Panel lecture. In Proceedings of the XXV Convegno Nazionale di Geotecnica, La Geotecnica nella Difesa del Territorio e delle Infrastrutture dalle Calamità Naturali', Baveno, Italy, 4–6 June 2014; pp. 167–186.
10. Cotecchia, F.; Santaloia, F.; Lollino, P.; Vitone, C.; Pedone, G.; Bottiglieri, O. From a phenomenological to a geomechanical approach to landslide hazard analysis. *Eur. J. Environ. Civ. Eng.* **2016**, *20*, 1004–1031. [CrossRef]
11. Cotecchia, F.; Tagarelli, V.; Vitone Cafaro, F.; Bottiglieri, O.; Guglielmi, S.; Petti, R.; Santaloia, F.; Lollino, P. *A Geo-Hydro-Mechanical Approach to Landslide Hazard Assessment and Mitigation: A Successful Application in Southern Italy*. Contributing Paper to GAR 2019. 2019. Available online: https://www.preventionweb.net/files/65782_f201cotecchiaetalgeohydromechanical.pdf (accessed on 21 September 2020).
12. Picarelli, L. Conoscere per prevedere (dall'equilibrio limite alla meccanica dei pendii). *Riv. Ital. Geotec.* **2009**, *4*, 51–68.
13. Cascini, L. Criteri di analisi e gestione del rischio da frana: Dal Governo centrale alle comunità locali. Relazione Generale. La geotecnica nella difesa del territorio e delle infrastrutture dalle calamità naturali. In Proceedings of the XXV Italian Geotechnical Congress, Baveno, Italy, 4–6 June 2014; AGI: Roma, Italy, 2014; pp. 103–150.
14. Varnes, D.J. Slope movement types and processes. In *Special Report 176: Landslides: Analysis and Control, Transportation and Road Research Board*; Schuster, R.L., Krizek, R.J., Eds.; National Academy of Science: Washington, DC, USA, 1978; pp. 11–33.
15. Hutchinson, J.N. Morphological and geotechnical parameters of landslides in relation to geology and hydrogeology. In Proceedings of the 5th International Conference on Landslides, Lausanne, Switzerland, 10–15 July 1988; Volume 1, pp. 3–35.
16. Cruden, D.M.; Varnes, D.J. Landslide Types and Processes. In *Landslide-Investigation and Mitigation*; Turner, A.K., Schuster, R.L., Eds.; Transportation Research Board, Special Report n. 247; National Research Council: Washington, DC, USA, 1996; pp. 36–75.
17. Terzaghi, K. Mechanism of landslides. In *Application of Geology to Engineering Practice*; Paige, S., Ed.; Berkey Volume; Geological Society of America: Boulder, CO, USA, 1950; pp. 83–123.
18. van Westen, C.J.; Castellanos, E.; Kuriakose, S.L. Spatial data for landslide susceptibility, hazard, and vulnerability assessment: An overview. *Eng. Geol.* **2008**, *102*, 112–131. [CrossRef]

19. Herrera, G.; Mateos, R.M.; García-Davalillo, J.C.; Grandjean, G.; Poyiadji, E.; Maftei, R.; Filipciuc, T.C.; Auflič, M.J.; Jež, J.; Podolszki, L.; et al. Landslide databases in the geological surveys of Europe. *Landslides* **2018**, *15*, 359–379. [CrossRef]
20. Elia, G.; Cotecchia, F.; Pedone, G.; Vaunat, J.; Vardon, P.J.; Pereira, C.; Springman, S.; Rouainia, M.R.; Esch, J.V.; Koda, E.; et al. Numerical modelling of slope-vegetation-atmosphere interaction: An overview. *Q. J. Eng. Geol. Hydrogeol.* **2017**, *50*, 249–270. [CrossRef]
21. Leroueil, S.; Vaunat, J.; Picarelli, L.; Locat, J.; Faure, R.; Lee, H. A geotechnical characterisation of slope movements. In Proceedings of the 7th International Symposium on Landslides, Trondheim, Norway, 17–21 June 1996; Volume 1, pp. 53–74.
22. Potts, D.M.; Zdravkovic, L. *Finite Element Analysis in Geotechnical Engineering: Theory*; Thomas Telford: London, UK, 1999.
23. Olivella, S.; Gens, A.; Carrera, J.; Alonso, E.E. Numerical formulation for a simulator (CODE_BRIGHT) for the coupled analysis of saline media. *Eng. Comput.* **1996**, *13*, 87–112. [CrossRef]
24. Cundall, P.A.; Strack, O.D. A discrete numerical model for granular assemblies. *Géotechnique* **1979**, *29*, 47–65. [CrossRef]
25. Sulsky, D.; Chen, Z.; Schreyer, H.L. A particle method for history-dependent materials. *Comput. Methods Appl. Mech. Eng.* **1994**, *118*, 179–196. [CrossRef]
26. Soga, K.; Alonso, E.E.; Yerro, A.; Kumar, K.; Bandara, S. Trends in large-deformation analysis of landslide mass movements with particular emphasis on the material point method. *Géotechnique* **2016**, *66*, 248–273. [CrossRef]
27. Biot, M.A. General theory of three-dimensional consolidation. *J. Appl. Phys.* **1941**, *12*, 155–164. [CrossRef]
28. Fredlund, D.G.; Rahardjo, H. *Soil Mechanics for Unsaturated Soils*; John Wiley & Sons: New York, NY, USA, 1993.
29. Bjerrum, L. *Progressive Failure in Slopes of Overconsolidated Plastic Clay and Clay Shales*; Norwegian Geotechnical Institute: Oslo, Norway, 1967.
30. Bishop, A.W. The Influence of Progressive Failure on the Choice of the Method of Stability Analysis. *Géotechnique* **1971**, *21*, 168–172. [CrossRef]
31. Chandler, R.J.; Skempton, A.W. The design of permanent cutting slopes in stiff fissured clays. *Géotechnique* **1974**, *24*, 457–466. [CrossRef]
32. Morgenstern, N.R. Managing risk in Geotechnical Engineering. Third Casagrande Lecture. In Proceedings of the 10th Pan-American Conference on Soil Mechanics and Foundation Engineering, Guadalajara, Mexico, 29 October–3 November 1995; Volume 4, pp. 102–126. Available online: http://www.barbau.ca/content/managing-risk-geotechnical-engineering-third-casagrande-lecture (accessed on 7 November 2020).
33. Duncan, J.M. State of the art: Limit equilibrium and finite-element analysis of slopes. *J. Geotech. Eng.* **1996**, *122*, 577–596. [CrossRef]
34. Gens, A.; Alonso, E.E. Aznalcóllar dam failure. Part 2: Stability conditions and failure mechanism. *Géotechnique* **2006**, *56*, 185–201. [CrossRef]
35. Picarelli, L.; Olivares, L. Mechanical behaviour of highly fissured sheared clay shales. In Proceedings of the Advances in Geotechnical Engineering: The Skempton Conference, London, UK, 29–31 March 2004; Volume 1, pp. 580–591.
36. Picarelli, L.; Russo, C. Remarks on the mechanics of slow active landslides and the interaction with man-made works. In *Landslides: Evaluation and Stabilization, Proceedings of the 9th International Symposium on Landslides, Rio de Janeiro, Brazil, 28 June–2 July 2004*; Lacerda, W.A., Ehrlich, M., Fontoura, S.A.B., Sayao, A.S.F.J., Eds.; Balkema: Rotterdam, The Netherlands, 2004; Volume 2, pp. 1141–1176.
37. Alonso, E.E.; Pinyol, N.M. Criteria for rapid sliding I. A review of Vaiont case. *Eng. Geol.* **2010**, *114*, 198–210. [CrossRef]
38. Lollino, P.; Santaloia, F.; Amorosi, A.; Cotecchia, F. Delayed failure of quarry slopes in stiff clays: The case of the Lucera landslide. *Géotechnique* **2011**, *61*, 861–874. [CrossRef]
39. Carey, J.M.; Petley, D.N. Progressive shear-surface development in cohesive materials; implications for landslide behavior. *Eng. Geol.* **2014**, *177*, 54–65. [CrossRef]
40. Cotecchia, F.; Pedone, G.; Bottiglieri, O.; Santaloia, F.; Vitone, C. Slope-atmosphere interaction in a tectonized clayey slope: A case study. *Riv. Ital. Geotec.* **2014**, *48*, 34–36.
41. Cotecchia, F.; Vitone, C.; Santaloia, F.; Pedone, G.; Bottiglieri, O. Slope instability processes in intensely fissured clays: Case histories in the Southern Apennines. *Landslides* **2015**, *12*, 877–893. [CrossRef]

42. Hungr, O.; Evans, S.G.; Bovis, M.J.; Hutchinson, J.N. A review of the classification of landslides of the Flow Type. *Environ. Eng. Geosci.* **2001**, *7*, 221–238. [CrossRef]
43. Hungr, O.; McDougall, S.; Bovis, M. Entrainment of material by debris flows. In *Debris-Flow Hazards and Related Phenomena*; Jakob, M., Hungr, O., Eds.; Springer: Berlin/Heidelberg, Germany, 2005; pp. 135–158.
44. Cascini, L.; Cuomo, S.; Pastor, M.; Sorbino, G. Modeling of rainfall-induced shallow landslides of the flow-type. *J. Geotech. Geoenviron. Eng.* **2010**, *136*, 85–98. [CrossRef]
45. *Landslides in Sensitive Clays—From Research to Implementation*; Thakur, V.; L'Heureux, J.-S.; Locat, A. (Eds.) Advances in Natural and Technological Hazards Research; Springer: Berlin/Heidelberg, Germany, 2017.
46. Losacco, N.; Viggiani, G.M.B. Class A prediction of mechanised tunnelling in Rome. *Tunn. Undergr. Space Technol.* **2019**, *87*, 160–173. [CrossRef]
47. Bicanic, N. Discrete Element Methods. In *Encyclopedia of Computational Mechanics*; Part 1., Fundametals; Stein, E., de Borst, R., Hughes, T.J.R., Eds.; Wiley: Hoboken, NJ, USA, 2004; pp. 311–337.
48. Calvetti, F. Discrete modelling of granular materials and geotechnical problems. *Eur. J. Environ. Civ. Eng.* **2008**, *12*, 951–965. [CrossRef]
49. Gabrieli, F.; Pol, A.; Thoeni, K. Comparison of two DEM strategies for modelling cortical meshes. In Proceedings of the 5th International Conference on Particle-Based Methods—Fundamental and Applications, Hannover, Germany, 26–28 September 2017; pp. 489–496.
50. O'Sullivan, C. *Particulate Discrete Element Modelling—A Geomechanics Perspective*; Applied Geotechnics; Routledge: Abingdon, UK, 2017; Volume 4, pp. 1–576.
51. Takeda, H.; Miyama, S.M.; Sekiya, M. Numerical simulation of viscous flow by smoothed particle hydrodynamics. *Prog. Theor. Phys.* **1994**, *92*, 939–960. [CrossRef]
52. Liu, G.R.; Liu, M.B. *Smoothed Particle Hydrodynamics: A Meshfree Particle Method*; World Scientific Publishing Company: Singapore, 2003.
53. Blanc, T.; Pastor, M. A stabilized fractional step. Runge–Kutta Taylor SPH algorithm for coupled problems in geomechanics. *Comput. Methods Appl. Mech. Eng.* **2012**, *221*, 41–53. [CrossRef]
54. Blanc, T.; Pastor, M. A stabilized Runge–Kutta, Taylor smoothed particle hydrodynamics algorithm for large deformation problems in dynamics. *Int. J. Numer. Methods Eng.* **2012**, *91*, 1427–1458. [CrossRef]
55. Cuomo, S.; Pastor, M.; Capobianco, V.; Cascini, L. Modelling the space–time evolution of bed entrainment for flow-like landslides. *Eng. Geol.* **2016**, *212*, 10–20. [CrossRef]
56. Sayed, M.; Savage, S.B. Rapid gravity flow of cohesionless granular materials down inclined chutes. *Z. Angew. Math. Phys.* **1983**, *34*, 84–100. [CrossRef]
57. Savage, S.B.; Hutter, K. The motion of a finite mass of granular material down a rough incline. *J. Fluid Mech.* **1989**, *199*, 177–215. [CrossRef]
58. Jenkins, J.T.; Askari, E. Hydraulic theory for a debris flow supported on a collisional shear layer. *CHAOS* **1999**, *9*, 654–658. [CrossRef] [PubMed]
59. Cafaro, F.; Cotecchia, F.; Santaloia, F.; Vitone, C.; Lollino, P.; Mitaritonna, G. Landslide hazard assessment and judgment of reliability: A geomechanical approach. *Bull. Eng. Geol. Environ.* **2017**, *76*, 397–412, Enhanced landslide investigations through advanced. [CrossRef]
60. Cotecchia, F.; Lenti, V.; Bottiglieri, O.; Cafaro, F. Analysis of a delayed re-activation of movements on a stiff clay slope in Southern Italy after foot excavation. In *Landslides: Evaluation and Stabilization; Proceedings of the 9th International Symposium on Landslides, Rio de Janeiro, Brazil, 28 June–2 July 2004*; Lacerda, W.A., Ehrlich, M., Fontoura, S.A.B., Sayao, A.S.F.J., Eds.; Balkema: Rotterdam, The Netherlands, 2004; Volume 2, pp. 1207–1214.
61. Cotecchia, F.; Tagarelli, V.; Pedone, G.; Ruggieri, G.; Guglielmi, S.; Santaloia, F. Analysis of climate-driven processes in clayey slopes for early warning system design. *Proc. Inst. Civ. Eng. Geotech. Eng.* **2019**, *172*, 465–480. [CrossRef]
62. Allen, R.G.; Pereira, L.S.; Raes, D.; Smith, M. *Crop Evapo-Transpiration (Guidelines for Computing Crop Water Requirements)*; Irrigation and Drainage Paper 56; Food and Agriculture Organization of the United Nations: Rome, Italy, 1998.
63. Pedone, G.; Ruggieri, G.; Trizzino, R. Characterisation of climatic variables used to identify instability thresholds in clay slopes. *Géotech. Lett.* **2018**, *8*, 231–239. [CrossRef]
64. Tagarelli, V. Analysis of the Slope-Vegetation-Atmosphere Interaction for the Design of the Mitigation Measures of Landslide Risk in Clayey Slopes. Ph.D. Thesis, Politecnico di Bari, Bari, Italy, 2019.

65. Tagarelli, V.; Cotecchia, F. Deep Movements in Clayey Slopes Relating to Climate: Modeling for Early Warning System Design. *Lect. Notes Civ. Eng.* **2020**, *40*, 205–214.
66. Pedone, G. Interpretation of Slow and Deep Landslides Triggered by Slope-Atmosphere Interaction in Slopes Formed of Fissured Clayey Turbidites. Ph.D. Thesis, Politecnico di Bari, Bari, Italy, 2014.
67. Tagarelli, V.; Cotecchia, F. The effects of slope initialization on the numerical model predictions of the slope-vegetation-atmosphere interaction. *Geosciences* **2020**, *10*, 85. [CrossRef]
68. Guerricchio, A.; Melidoro, G.; Panaro, V. Deformazioni gravitative dei versanti nel territorio comunale di Tolve (Basilicata). *Boll. Della Soc. Geol. Ital.* **2000**, *119*, 613–622.
69. Kovacevic, K.; Potts, D.M.; Vaughan, P.R. Progressive failure in clay embankment due to seasonal climate changes. In Proceedings of the 5th International Conference on Soil Mechanics and Geotechnical Engineering, Istanbul, Turkey, 27–31 August 2001; Volume 3, pp. 2127–2130.
70. Rouainia, M.; Davies, O.; O'Brien, A.; Glendinning, S. Numerical modelling of climate effects on slope stability. *Eng. Sustain.* **2009**, *162*, 81–89. [CrossRef]
71. Askarinejad, A.; Casini, F.; Bischof, P.; Beck, A.; Springman, S.M. Rainfall induced instabilities: A field experiment on a silty sand slope in northern Switzerland. *Riv. Ital. Geotec.* **2012**, *46*, 50–71.
72. Troncone, A.; Conte, E.; Donato, A. Two and three-dimensional numerical analysis of the progressive failure that occurred in an excavation-induced landslide. *Eng. Geol.* **2014**, *183*, 265–275. [CrossRef]
73. Troncone, A.; Conte, E.; Donato, A. Three-dimensional finite element analysis of the Senise landslide. *Procedia Eng.* **2016**, *158*, 212–217. [CrossRef]
74. Locat, A.; Locat, P.; Demers, D.; Leroueil, S.; Robitaille, D.; Lefebvre, G. The Saint-Jude landslide of 10 May 2010, Quebec, Canada: Investigation and characterization of the landslide and its failure mechanism. *Can. Geotech. J.* **2017**, *54*, 1357–1374. [CrossRef]
75. Sitarenios, P.; Casini, F.; Askarinejad, A.; Springman, S. Hydro-mechanical analysis of a surficial landslide triggered by artificial rainfall: The Ruedlingen field experiment. *Géotechnique* **2019**. [CrossRef]
76. Scuro, M. Analisi Quantitativa di un Processo di Riattivazione di Frana Conseguente ad uno Scavo al Piede del Pendio "Quantitative Analysis of the Reactivation of a Landslide Process Induced by Foot Excavation of a Slope". Master's Thesis, Technical University of Bari, Bari, Italy, 2003.
77. Hungr, O.; Leroueil, S.; Picarelli, L. The Varnes classification of landslide types, an update. *Landslides* **2014**, *11*, 167–194. [CrossRef]
78. Hutchinson, J.N. The reponse of London clay cliffs to differing rates of toe erosion. *Geol. Appl. Idrogeol.* **1973**, *8*, 221–239.
79. Dixon, N.; Bromhead, E.N. Landsliding in London Clay Coastal Cliffs. *Quaterly J. Eng. Geol.* **2002**, *35*, 327–343. [CrossRef]
80. Cotecchia, F.; Santaloia, F.; Bottiglieri, O.; Monterisi, L. Landslides in stiff clay slopes along the Adriatic coast (Central Italy). In Proceedings of the X International Symposium on Landslide, Xi'an, China, 30 June–4 July 2008; Volume 2, pp. 1525–1531.
81. Santaloia, F.; Cotecchia, V.; Monterisi, L. Geological evolution and landslide mechanisms along the central Adriatic coastal slopes. In Proceedings of the Advances in Geotechnical Engineering: The Skempton Conference, London, UK, 29–31 March 2004; Volume 2, pp. 943–954.
82. Cotecchia, V. La Grande frana di Ancona. In Proceedings of the Convegno Dell'accademia Nazionale dei Lincei: "La Stabilità del Suolo in Italia: Zonazione della Sismicità, Frane", Rome, Italy, 30–31 May 1996; pp. 187–259.
83. Cooper, M.R.; Bromhead, E.N.; Petley, D.J.; Grant, D.I. The Selborne cutting stability experiment. *Géotechnique* **1998**, *48*, 83–101. [CrossRef]
84. Cotecchia, F.; Chandler, R.J. The influence of structure on the pre-failure behaviour of a natural clay. *Géotechnique* **1997**, *47*, 523–544. [CrossRef]
85. Hight, D.W.; Gasparre, A.; Nishimura, S.; Minh, N.A.; Jardine, R.J.; Coop, M.R. Characteristics of the London Clay from the Terminal 5 site at Heathrow Airport. *Géotechnique* **2007**, *57*, 3–18. [CrossRef]
86. Wood, D.M.; Jendele, L.; Chan, A.H.C.; Cooper, M.R. Slope failure by pore pressure recharge: Numerical analysis. In Proceedings of the 11th European Conference on Soil Mechanics and Foundation Engineering, Copenhagen, Denmark, 28 May–1 June 1995; Volume 6, pp. 1–8.
87. Chandler, R.J.; Leroueil, S.; Trenter, N.A. Measurements of the permeability of London Clay using a self-boring permeameter. *Géotechnique* **1990**, *40*, 113–124. [CrossRef]

88. Dewhurst, D.N.; Aplin, A.C.; Sarda, J.-P.; Yang, Y. Compaction-driven evolution of porosity and permeability in natural mudstones: An experimental study. *J. Geophys. Res. Solid Earth* **1998**, *103*, 651–661. [CrossRef]
89. Holmsen, G. Landslips in Norwegian quick clays. *Géotechnique* **1953**, *3*, 187–194. [CrossRef]
90. Bjerrum, L. Stability of natural slopes in quick clay. *Géotechnique* **1955**, *5*, 101–119. [CrossRef]
91. L'Heureux, J.S. A study of the retrogressive behaviour and mobility of Norwegian quick clay landslides. In *Landslides and Engineered Slopes—Protecting Society through Improved Understanding*; Eberhardt, E., Froese, C., Turner, A.K., Leroueil, S., Eds.; CRC Press: London, UK, 2012; Volume 1, pp. 981–988.
92. *Landslides in Sensitive Clays—From Geosciences to Risk Management*; L'Heureux, J.-S.; Locat, A.; Leroueil, S.; Demers, D.; Locat, J. (Eds.) Advances in Natural and Technological Hazards Research; Springer: Berlin/Heidelberg, Germany, 2014; Volume 36.
93. Locat, A.; Leroueil, S.; Bernander, S.; Demers, D.; Jostad, H.P.; Ouehb, L. Progressive failures in Eastern Canadian and Scandinavian sensitive clays. *Can. Geotech. J.* **2011**, *48*, 1696–1712. [CrossRef]
94. Locat, A.; Leroueil, S.; Fortin, A.; Demers, D.; Jostad, H.P. The 1994 landslide at Sainte-Monique, Quebec: Geotechnical investigation and application of progressive failure analysis. *Can. Geotech. J.* **2015**, *52*, 490–504. [CrossRef]
95. Locat, A.; Demers, D.; Leroueil, S. Spreads in Canadian sensitive clays. In Proceedings of the 12th International Symposium on Landslides and Engineered Slopes, Experience, Theory and Practice, Napoli, Italy, 12–19 June 2016; Volume 2, pp. 1295–1304.
96. Skempton, A.W.; Northey, R.D. Sensitivity of clays. *Géotechnique* **1952**, *3*, 40–51.
97. Torrance, J.K. Towards a general model of quick clay development. *Sedimentology* **1983**, *30*, 547–555. [CrossRef]
98. Lefebvre, G. Sensitive Clays of Eastern Canada: From Geology to Slope Stability. In *Landslides in Sensitive Clays*; Thakur, V., L'Heureux, J.-S., Locat, A., Eds.; Advances in Natural and Technological Hazards Research; Springer: Berlin/Heidelberg, Germany, 2017; Volume 40, pp. 15–34.
99. Lefebvre, G. Soft sensitive clays. In *Landslides Investigation and Mitigation*; Turner, A.K., Schuster, R.L., Eds.; Special Report 247; Transportation Research Board, National Research Council, National Academy Press: Washington, DC, USA, 1996; pp. 607–619.
100. Tavenas, F. Landslides in Canadian sensitive clays—A state-of-the-art. In Proceedings of the 4th International Symposium on Landslides, Toronto, ON, Canada, 16–21 September 1984; pp. 141–153.
101. Zhang, X.; Sheng, D.; Sloan, S.W.; Bleyer, J. Lagrangian modelling of large deformation induced by progressive failure of sensitive clays with elastoviscoplasticity. *Int. Numer. Methods Eng.* **2017**, *112*, 963–989. [CrossRef]
102. Demers, D.; Robitaille, D.; Locat, P.; Potvin, J. Inventory of Large Landslides in Sensitive Clay in the Province of Québec, Canada: Preliminary Analysis. In *Landslides in Sensitive Clays*; Springer: Berlin/Heidelberg, Germany, 2014.
103. Del Prete, M.; Hutchinson, J.N. La frana di Senise del 26-7-1986 nel quadro morfologico del versante meridionale della collina Timpone. *Riv. Ital. Geotec.* **1988**, *22*, 7–34.
104. Guerricchio, A.; Melidoro, G. Urbanizzazione e franosità delle formazioni sabbiose plio-pleistoceniche in Basilicata: Il caso di Senise. *Mem. Soc. Geol. Ital.* **1988**, *37*, 745–774.
105. Cotecchia, V.; Grassi, D.; Sdao, F. Evoluzione geomorfologica e movimenti di massa del versante vallivo impegnato dall'abitato di Senise (Basilicata). *Geol. Appl. Idrogeol.* **1989**, *24*, 1–25.
106. Troncone, A. Numerical analysis of a landslide in soils with strain-softening behavior. *Géotechnique* **2005**, *55*, 585–596. [CrossRef]
107. Zhang, X.; Wang, L.; Krabbenhoft, K.; Tinti, S. A case study and implication: Particle finite element modelling of the 2010 Saint-Jude sensitive clay landslide. *Landslides* **2019**. [CrossRef]
108. Pellegrino, A.; Ramondini, M.; Russo, C.; Urciuoli, G. Kinematic features of earthflows in Southern Apennines. In Proceedings of the 8th International Symposium on Landslides, Cardiff, UK, 26–30 June 2000; Volume 2, pp. 1195–2002.
109. Picarelli, L. Mechanisms and rates of slope movements in fine grained soils. In Proceedings of the GeoEng2000 International ISSMGE-ISRM-IMEG Conference on Geotechnical and Geological Engineering, Melbourne, Australia, 19–24 November 2000; pp. 1618–1670.
110. Picarelli, L.; Urciuoli, G.; Ramondini, L.; Comegna, L. Main features of mudslides in tectonized highly fissured clay shales. *Landslides* **2005**, *2*, 15–30. [CrossRef]
111. Bertolini, G.; Guida, M.; Pizziolo, M. Landslides in Emilia-Romagna region (Italy): Strategies for hazard assessment and risk management. *Landslides* **2005**, *2*, 302–312. [CrossRef]

112. Ronchetti, F.; Borgatti, L.; Cervi, F.; Lucente, C.C.; Veneziano, M.; Corsini, A. The Valoria landslide reactivation in 2005–2006 (Northern Apennines, Italy). *Landslides* **2007**, *4*, 189–195. [CrossRef]
113. Comegna, L.; Picarelli, L.; Urciuoli, G. The mechanics of mudslides as a cyclic undrained-drained process. *Landslides* **2007**, *4*, 217–232. [CrossRef]
114. Di Maio, C.; Vassallo, R.; Vallario, M.; Pascale, S.; Sdao, F. Structure and kinematics of a landslide in a complex clayey formation of the Italian Southern Apennines. *Eng. Geol.* **2010**, *116*, 311–322. [CrossRef]
115. Guerriero, L.; Coe, J.A.; Revellino, P.; Grelle, G.; Pinto, F.; Guadagno, F.M. Influence of slip-surface geometry on earth-flow deformation, Montaguto earth flow, southern Italy. *Geomorphology* **2014**, *219*, 285–305. [CrossRef]
116. Urciuoli, G.; Comegna, L.; Di Maio, C.; Picarelli, L. The Basento Valley: A natural laboratory to understand the mechanics of earthflows. *Riv. Ital. Geotec.* **2016**, *50*, 71–90.
117. Santaloia, F.; Cotecchia, F.; Polemio, M. Mechanics of a tectonized soil slope: Influence of boundary conditions and rainfalls. *Q. J. Eng. Geol.* **2001**, *34*, 165–185. [CrossRef]
118. Mezzina, G. Interpretazione della Pericolosità da Frana nel Centro Abitato di Motta Montecorvino (FG). Master's Thesis, Politecnico di Bari, Bari, Italy, 2007.
119. Vassallo, R.; Grimaldi, G.M.; Di Maio, C.; Di Nocera, S. An earthflow in structurally complex formations of the Italian Southern Apennines: Geological structure and kinematics. In Proceedings of the 12th International Symposium on Landslides and Engineered Slopes, Experience, Theory and Practice, Napoli, Italy, 12–19 June 2016; Volume 3, pp. 1979–1986.
120. Vassallo, R.; Doglioni, A.; Grimaldi, G.M.; Di Maio, C.; Simeone, V. Relationships between rain and displacements of an active earthflow: A data-driven approach by EPRMOGA. *Nat. Hazards* **2016**, *81*, 1467–1482. [CrossRef]
121. Giordan, D.; Allasia, P.; Manconi, A.; Baldo, M.; Santangelo, M.; Cardinali, M.; Corazza, A.; Albanese, V.; Lollino, G.; Guzzetti, F. Morphological and kinematic evolution of a large earthflow: The Montaguto landslide, southern Italy. *Geomorphology* **2013**, *187*, 61–79. [CrossRef]
122. Lollino, P.; Giordan, D.; Allasia, P. The Montaguto earthflow: A back-analysis of the process of landslide propagation. *Eng. Geol.* **2014**, *170*, 66–79. [CrossRef]
123. Cotecchia, V.; Del Prete, M.; Federico, A.; Fenelli, G.B.; Pellegrino, A.; Picarelli, L. Studio di una colata attiva in formazioni strutturalmente complesse presso Brindisi di Montagna Scalo (PZ). In Proceedings of the XVI Convegno Nazionale Geotecnica, Bologna, Italy, 14–16 May 1986; pp. 253–264.
124. Picarelli, L. Modellazione e monitoraggio di una colata in formazioni strutturalmente complesse. In Proceedings of the Convegno su Cartografia e Monitoraggio dei Movimenti Franosi, Bologna, Italy, 10–11 November 1988; pp. 119–130.
125. Bentivenga, M.; Grimaldi, S.; Palladino, G. Caratteri geomorfologici della instabilità del versante sinistro del Fiume Basento. *Giomale Geol. Appl.* **2006**, *4*, 123–130.
126. Guerriero, G. Modellazione Sperimentale del Comportamento Meccanico dei Terreni in Colata. Ph.D. Thesis, Università di Napoli Federico II, Napoli, Italy, 1995.
127. Picarelli, L.; Russo, C.; Urciuoli, G. Modelling earthflows based on experiences. In Proceedings of the 11th European Conference on Soil Mechanics and Foundation Engineering: The interplay between Geotechnical Engineering and Engineering Geology, Copenhagen, Denmark, 12–16 August 1995; Volume 6, pp. 157–162.
128. Vassallo, R.; Grimaldi, G.; Di Maio, C. Pore water pressures induced by historical rain series in a clayey landslide: 3D modeling. *Landslides* **2014**. [CrossRef]
129. Urciuoli, G.; Pirone, M.; Comegna, L.; Picarelli, L. Long-term investigations on the pore pressure regime in saturated and unsaturated sloping soils. *Eng. Geol.* **2016**, *212*, 98–119. [CrossRef]
130. AGI. Some Italian experiences on the mechanical characterisation of structurally complex clay soils. In Proceedings of the 4th International Congress Society Rock Mechanics, Montreux, Switzerland, 2–8 September 1979; Volume 1, pp. 827–846.
131. Cotecchia, F.; Santaloia, F. Compression behaviour of structurally complex marine clays; Panel lecture. In Proceedings of the Nakase Memorial Symposium on "Soft Ground Engineering in Coastal Areas", Yokosuka, Japan, 28–29 November 2002; pp. 63–72.

132. Cotecchia, F.; Vitone, C.; Cafaro, F.; Santaloia, F. The mechanical behaviour of intensely fissured high plasticity clays from Daunia. In *Characterisation and Engineering Properties of Natural Soils, Proceedings of the 2nd Inter. Workshop, Singapore, 29 November–1 December 2006*; Taylor & Francis Group: London, UK, 2007; Volume 3–4, pp. 1975–2003.
133. Cotecchia, F.; Vitone, C. On the model requirements to predict the behaviour of fissured clays. In Proceedings of the XV ECSMGE, Atene, Greece, 11–15 September 2011; pp. 525–530.
134. Vitone, C.; Cotecchia, F. The influence of intense fissuring on the mechanical behaviour of clays. *Géotechnique* **2011**, *61*, 1003–1018. [CrossRef]
135. Vitone, C.; Cotecchia, F.; Federico, A.; Viggiani, G. On the geomechanical characterisation of complexities in clays. Experimental studies. *Riv. Ital. Geotec.* **2018**, *52*, 7–29.
136. Bilotta, E. Alcuni risultati da prove udometriche su argille a scaglie: Compressibilità e rigonfiamento. *Riv. Ital. Geotec.* **1984**, *3*, 52–66.
137. Olivares, L. Caratterizzazione dell'Argilla di Bisaccia in Condizioni Monotone, Cicliche e Dinamiche e Riflessi sul Comportamento del Colle a Seguito del Terremoto del 1980. Ph.D. Thesis, Università di Napoli Federico II, Napoli, Italy, 1997.
138. Picarelli, L.; Di Maio, C.; Olivares, L.; Urciuoli, G. Properties and behaviour of tectonised clay shales in Italy. In Proceedings of the 2nd International Symposium Geotechnics of Hard Soils–Soft Rocks, Naples, Italy, 12–14 October 1998; Volume 3, pp. 1211–1241.
139. Picarelli, L.; Olivares, L.; Di Maio, C.; Silvestri, F.; Di Nocera, S.; Urciuoli, G. Structure properties and mechanical behaviour of the highly plastic intensely fissured Bisaccia clay shale. In Proceedings of the International Symposium on Characterisation and Engineering Properties of Natural Soils, Singapore, 2–4 December 2002; Volume 2, pp. 947–962.
140. Vitone, C.; Cotecchia, F.; Viggiani, C. *Localisation Processes and Size Effects for Fissured Clay Specimens*; Springer Series in Geomechanics and Geoengineering; Springer: Berlin/Heidelberg, Germany, 2012.
141. Vitone, C.; Guglielmi, S.; Pedone, G.; Cotecchia, F. Effects of micro-to meso-features on the permeability of fissured clays. *Geotech. Lett.* **2019**, *9*, 369–376. [CrossRef]
142. Urciuoli, G. Permeabilità di argilliti a scaglie. In Proceedings of the Conferenza Il Ruolo dei Fluidi nei Problemi di Ingegneria Geotecnica, Mondovì, Italy, 6–7 September 1994; pp. I-185–I-204.
143. Di Maio, C.; De Rosa, J.; Vassallo, R.; Coviello, R.; Macchia, G. Hydraulic conductivity and pore water pressures in a clayey landslide: Experimental data. *Geosciences* **2020**, *10*, 102. [CrossRef]
144. Cotecchia, F.; Santaloia, F.; Santoro, F. Movements in a tectonized soil slope: Comparison of monitoring data and modelling results. In Proceedings of the GeoEng2000 International ISSMGE-ISRM-IMEG Conference on Geotechnical and Geological Engineering, Melbourne, Australia, 19–24 November 2000.
145. Pellegrino, A.; Picarelli, L.; Urciuoli, G. Experiences of mudslides in Italy. In Proceedings of the International Workshop on Occurrence and Mechanisms of Flow-Like Landslides in Natural Slopes and Earthfills, Sorrento, Patron, Bologna, Italy, 14–16 May 2004; pp. 191–206.
146. De Luca, V.; Mario, B.; Palladino, G.; Grimaldi, S.; Prosser, G. A finite element analysis of the Brindisi di Montagna Scalo earthflow. *Eng. Geol. Soc. Territ.* **2015**, *2*, 1239–1243.
147. Lollino, P.; Giordan, D.; Allasia, P.; Pastor, M. Analysis of the propagation of a large earthflow by SPH technique application. In Proceedings of the 12th International Symposium on Landslides and Engineered Slopes, Experience, Theory and Practice, Napoli, Italy, 12–19 June 2016; Volume 2, pp. 1313–1321.
148. Lollino, P.; Elia, G.; Cotecchia, F.; Mitaritonna, G. Analysis of landslide reactivation mechanisms in Daunia clay slopes by means of limit equilibrium and FEM methods. In Proceedings of the Geoflorida 2010: Advances in Analysis, Modelling and Design, West Palm Beach, FL, USA, 20–24 February 2010; pp. 3130–3139.
149. Lollino, P.; Cotecchia, F.; Elia, G.; Mitaritonna, G.; Santaloia, F. Interpretation of landslide mechanisms based on numerical modelling: Two case-histories. *Eur. J. Environ. Civ. Eng.* **2016**, *20*, 1032–1053. [CrossRef]
150. Cotecchia, F.; Vitone, C.; Petti, R.; Soriano, I.; Santaloia, F.; Lollino, P. Slow landslides in urbanised clayey slopes: An emblematic case from the south of Italy. Landslide damage assessment at the intermediate to small scale. In Proceedings of the 12th International Symposium on Landslides and Engineered Slopes, Experience, Theory and Practice, Napoli, Italy, 12–19 June 2016; Volume 2, pp. 691–698.
151. Capra, L.; Lugo-Hubp, J.; Borselli, L. Mass movements in tropical volcanic terrains: The case of Teziùtlan (Mexico). *Eng. Geol.* **2003**, *69*, 359–379. [CrossRef]

152. Ekanayake, J.C.; Philipps, C.J. Slope stability thresholds for vegetated hillslopes: A composite model. *Can. Geotech. J.* **2002**, *39*, 849–862. [CrossRef]
153. Cascini, L.; Cuomo, S.; Pastor, M. Inception of debris avalanches: Remarks on geomechanical modelling. *Landslides* **2013**, *10*, 701–711. [CrossRef]
154. Cascini, L.; Sorbino, G.; Cuomo, S.; Ferlisi, S. Seasonal effects of rainfall on the shallow pyroclastic deposits of the Campania region (southern Italy). *Landslides* **2014**, *11*, 779–792. [CrossRef]
155. Comegna, L.; Damiano, E.; Greco, R.; Guida, A.; Olivares, L.; Picarelli, L. Considerations on the failure of the Cervinara slope. In Proceedings of the 12th International Symposium on Landslides and Engineered Slopes, Experience, Theory and Practice, Napoli, Italy, 12–19 June 2016; Volume 2, pp. 663–670.
156. Olivares, L.; Picarelli, L. Shallow flowslides triggered by intense rainfalls on natural slopes covered by loose unsaturated pyroclastic soils. *Géotechnique* **2003**, *53*, 283–287. [CrossRef]
157. Pirone, M.; Papa, R.; Nicotera, M.V.; Urciuoli, G. In situ monitoring of the groundwater field in an unsaturated pyroclastic slope for slope stability evaluation. *Landslides* **2015**, *12*, 259–276. [CrossRef]
158. Sorbino, G.; Foresta, V. Unsaturated hydraulic characteristics of pyroclastic soils. In Proceedings of the 3rd International Conference on Unsaturated Soils, Recife, Brazil, 10–13 March 2002; Volume 1, pp. 405–410.
159. Sorbino, G.; Nicotera, M.V. Unsaturated soil mechanics in rainfall-induced flow landslides. *Eng. Geol.* **2013**, *165*, 105–132. [CrossRef]
160. Santo, A.; Di Crescenzo, G.; Forte, G.; Papa, R.; Pirone, M.; Urciuoli, G. Flow-type landslides in pyroclastic soils on flysch bedrock in southern Italy: The Bosco de' Preti case study. *Landslides* **2018**, *15*, 63–82. [CrossRef]
161. Ferlisi, S.; De Chiara, G.; Cascini, L. Quantitative risk analysis for hyperconcentrated flows in Nocera Inferiore (southern Italy). *Nat. Hazards* **2016**, *81*, 89–115. [CrossRef]
162. Take, W.A.; Bolton, M.D.; Wong, P.C.P.; Yeung, F.J. Evaluation of landslide triggering mechanisms in model fill slopes. *Landslides* **2004**, *1*, 173–184. [CrossRef]
163. Wang, F.W.; Sassa, K.; Wang, G. Mechanism of a long runout landslide triggered by the August 1998 heavy rainfall in Fukushima Prefecture, Japan. *Eng. Geol.* **2002**, *63*, 169–185. [CrossRef]
164. Lacerda, W.A. The behaviour of colluvial slopes in a tropical environment. In *Landslides: Evaluation and Stabilization, Proceedings of the 9th International Symposium on Landslides, Rio de Janeiro, Brazil, 28 June–2 July 2004*; Lacerda, W.A., Ehrlich, M., Fontoura, S.A.B., Sayao, A.S.F.J., Eds.; Balkema: Rotterdam, The Netherlands, 2004; Volume 2, pp. 1315–1342.
165. Fuchu, D.; Lee, C.F.; Sijing, W. Analysis of rainstorm induced slide-debris flows on natural terrain of Lantau Island, Hong Kong. *Eng. Geol.* **1999**, *51*, 279–290. [CrossRef]
166. Bilotta, E.; Cascini, L.; Foresta, V.; Sorbino, G. Geotechnical characterisation of pyroclastic soils involved in huge flowslides. *Geotech. Geol. Eng.* **2005**, *23*, 365–402. [CrossRef]
167. Damiano, E.; Olivares, L.; Picarelli, L. Steep-slope monitoring in unsaturated pyroclastic soils. *Eng. Geol.* **2012**, *137–138*, 1–12. [CrossRef]
168. Cascini, L.; Cuomo, S.; Guida, D. Typical source areas of May 1998 flow-like mass movements in the Campania region, Southern Italy. *Eng. Geol.* **2008**, *96*, 107–125. [CrossRef]
169. Damiano, E.; Olivares, L. The role of infiltration processes in steep slope stability of pyroclastic granular soils: Laboratory and numerical investigation. *Nat. Hazards* **2010**, *52*, 329–350. [CrossRef]
170. Pirone, M.; Damiano, E.; Picarelli, L.; Olivares, L.; Urciuoli, G. Groundwater-atmosphere interaction in unsaturated pyroclastic slopes at two sites in Italy. *Riv. Ital. Geotec.* **2012**, *3*, 29–49.
171. Greco, R.; Marino, P.; Santonastaso, G.F.; Damiano, E. Interaction between perched epikarst aquifer and unsaturated soil cover in the initiation of shallow landslides in pyroclastic soils. *Water* **2018**, *10*, 948. [CrossRef]
172. Cascini, L.; Cuomo, S.; Sorbino, G. Flow-like mass movements in pyroclastic soils: Remarks on the modelling of triggering mechanisms. *Riv. Ital. Geotec.* **2005**, *4*, 11–31.
173. Forte, G.; Pirone, M.; Santo, A.; Nicotera, M.V.; Urciuoli, G. Triggering and predisposing factors for flow-like landslides in pyroclastic soils: The case study of the Lattari Mts. (southern Italy). *Eng. Geol.* **2019**, *257*, 105137. [CrossRef]

174. Marino, P.; Peres, D.J.; Cancelliere, A.; Greco, R.; Bogaard, T.A. Soil moisture information can improve shallow landslide forecasting using the hydrometeorological threshold approach. *Landslides* **2020**, *17*, 2041–2054. [CrossRef]